Eosin Y-Derived Fluorescent Sensors: Selective Hg^{2+} Detection, and Targeted Biomedical Applications

Biplove Kumar[a], Venkatesh Muthukumar[b], Arnab Chakraborty[a], Asha Mahato[a], Balaram Ghosh[b]* and Neeladri Das[a]*

[a]*Department of Chemistry, Indian Institute of Technology Patna, Patna 801106 Bihar, India*

[b]*Epigenetic Research laboratory, Department of Pharmacy, Birla Institute of Technology and Science, Pilani, Hyderabad Campus, Jawahar Nagar, Kapra Mandal, Medchal District, Telangana 500078, India*

Corresponding authors: Balaram Ghosh (balaram@hyderabad.bits-pilani.ac.in) | Neeladri Das (neeladri@iitp.ac.in or neeladri2002@yahoo.co.in)

Table of Contents

1.1: Synthesis of **EY-S_O** and **EY-S_M**: Compounds **1** have been synthesized by following a protocol that has been reported earlier by our group[1]. **1** was used as synthons for the synthesis of **EY-S_O** and **EY-S_M** (Scheme 1). Initially, 1(438 mg, 0.7mmol) was reacted separately with o-bromobenzaldehyde (130 mg, 0.7mmol) and m-chlorobenzaldehyde (99 mg, 0.7mmol) in dry DMF under reflux for 12 h to form **EY-S_O** and **EY-S_M**, respectively. The resulting mixture was dried under vacuum and purified by column chromatography over silica gel using 20% ethyl acetate and hexane. **EY-S_O Yield (72%)** ^{1}H NMR (500 MHz, DMSO-d_6) δ (ppm): 10.59 (2H, S, -OH), 8.93 (1H, s, imine-H**),** 8.14 (1H, d, Ar-H), 7.90 (1H, d, Ar-H), 7.79 (1H, d, Ar-H), 7.62 (1H, d, Ar-H), 7.51 (1H, t, Ar-H), 7.29 (1H, d, Ar-H), 6.78 (2H, s, Ar-H). **EY-S_M (74%):** ^{1}H NMR (500 MHz, DMSO-D_6) δ (ppm): 8.93 (s, 1H), 8.73 (d, J = 2.3 Hz, 1H), 8.38 (d, J = 8.2 Hz, 1H), 8.33 (d, J = 7.8 Hz, 1H), 7.88 (d, J = 6.1 Hz, 1H), 7.83 (t, J = 8.0 Hz, 1H), 7.64 – 7.61 (d, 2H), 7.28 (d, J = 8.6 Hz, 1H), 6.78 (s, 2H).

1.2: Synthesis of **EY-M_O** and **EY-M_M :** (170 mg, 0.2 mmol) of **EY-S_O** and (153 mg, 0.2 mmol) **EY-S_M** was added separately to $Hg(OAc)_2$ (89 mg, 0.28 mmol) in 2 mL ethanol-water (1:1 v/v) mixture and stirred for 2 min to form **EY-M_O** and respectively. The precipitate was dried and collected after recrystallisation. **EY-M_O Yield (97%)** ^{1}H NMR (500 MHz, DMSO-d_6) δ (ppm): 10.21 (1H, S, -OH), 8.89 (1H, s, imine-H**),** 7.99 (1H, d, Ar-H), 7.70 (1H, d, Ar-H), 7.62 (1H, d, Ar-H), 7.55 (1H, d, Ar-H), 7.34 (1H, t, Ar-H), 7.30 (2H, d, Ar-H), 6.80 (2H, s, Ar-H), 1.93 (s, -OAc). **EY-M_M (94%) :** ^{1}H NMR (500 MHz, DMSO-d_6) δ (ppm): δ 8.93 (s, 1H), 8.72 (d, J = 4.2 Hz, 1H), 8.38 (d, J = 8.2 Hz, 1H), 8.33 (d, J = 7.8 Hz, 1H), 7.88 (d, J = 8.6 Hz, 1H), 7.83 (t, J = 8.0 Hz, 1H), 7.63 – 7.60 (d, 2H), 7.25 (d, J = 6.2 Hz, 1H), 6.76 (s, 2H), 1.93 (s, -OAc)

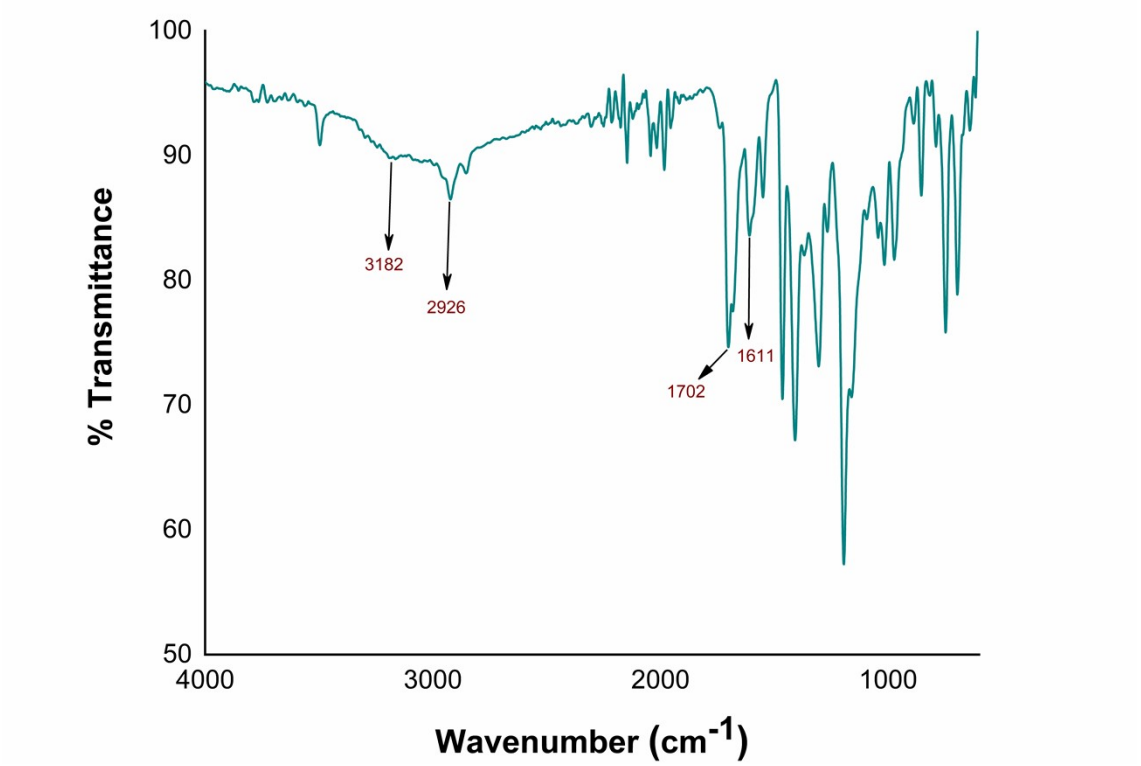

Fig. S1: IR spectrum of **EY-S_O**

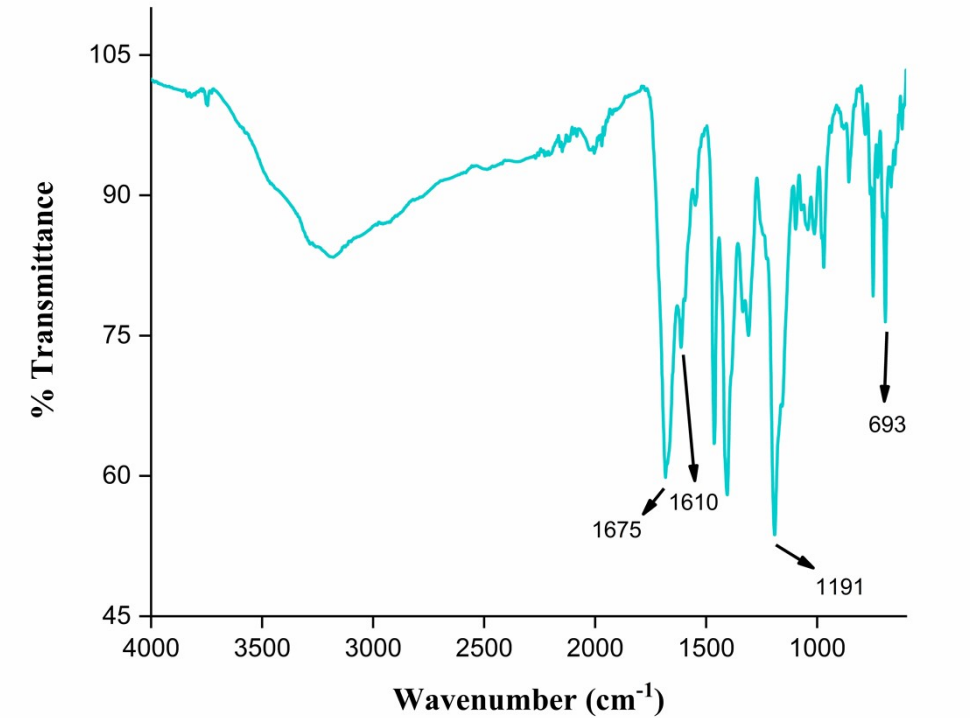

Fig. S2: IR spectrum of **EY-S_M**.

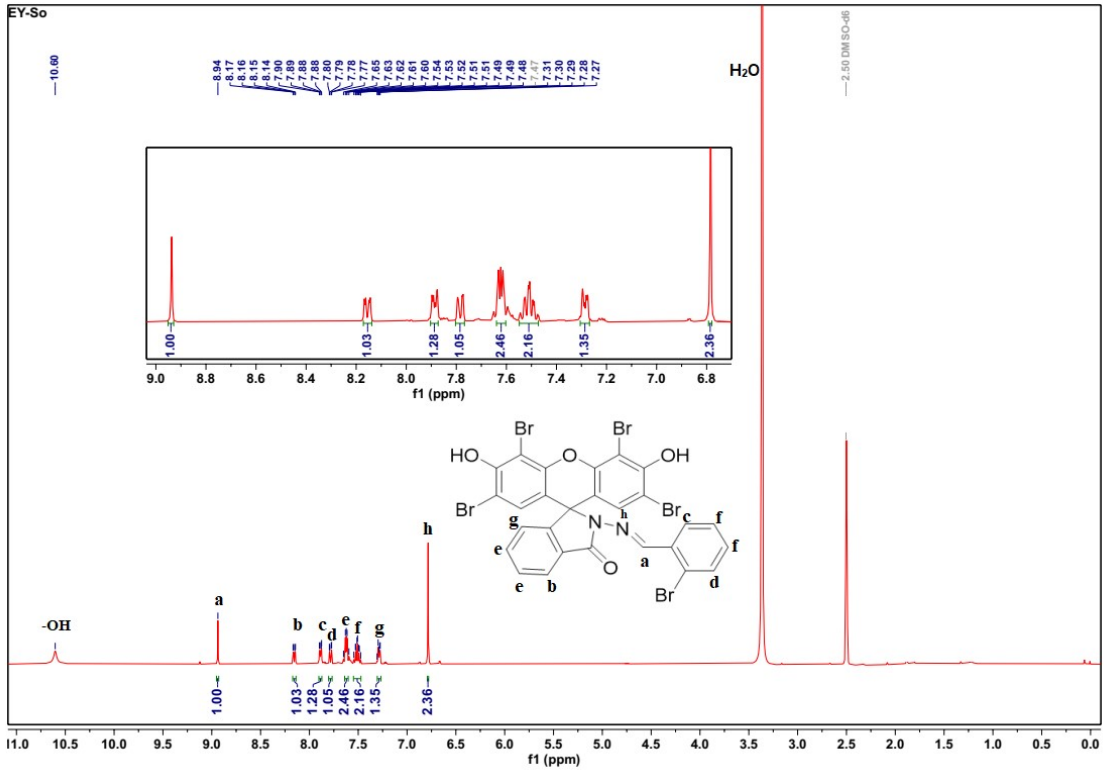

Fig. S3: ^{1}H NMR spectrum of **EY-S$_{O}$**.

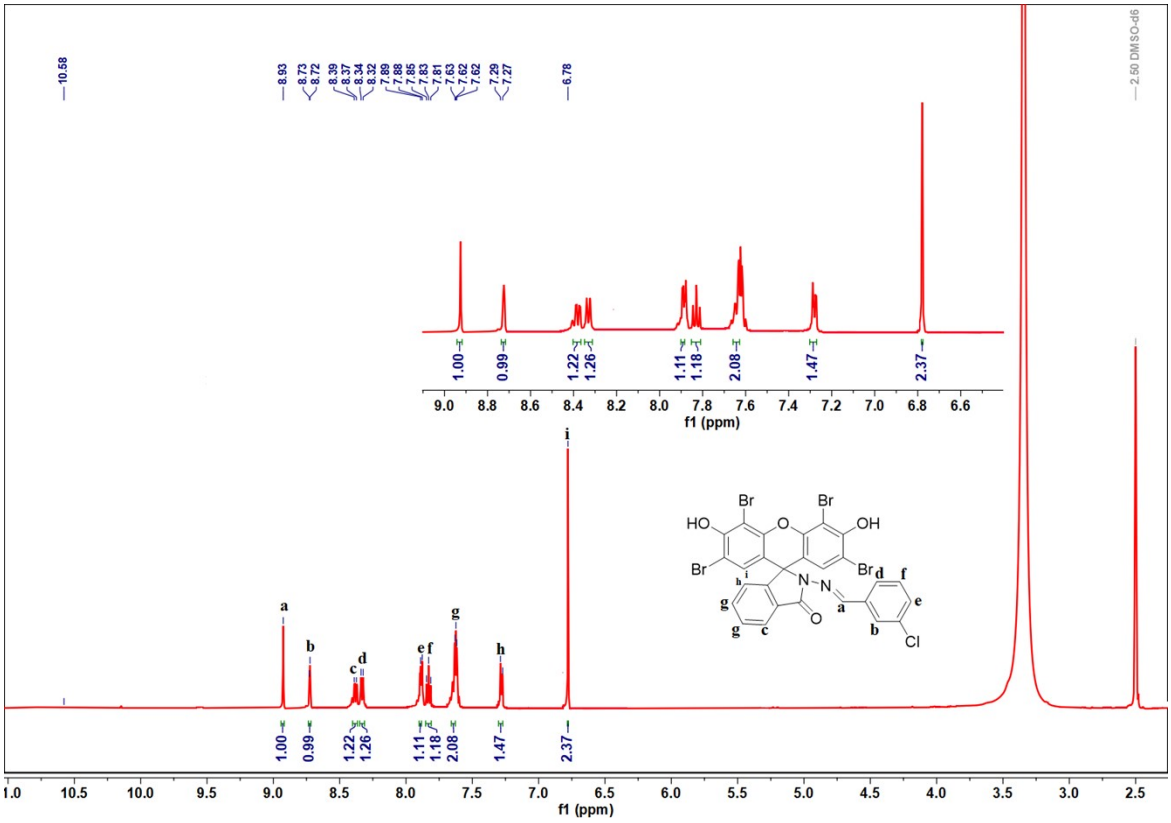

Fig. S4: ^{1}H NMR spectrum of **EY-S$_{M}$**.

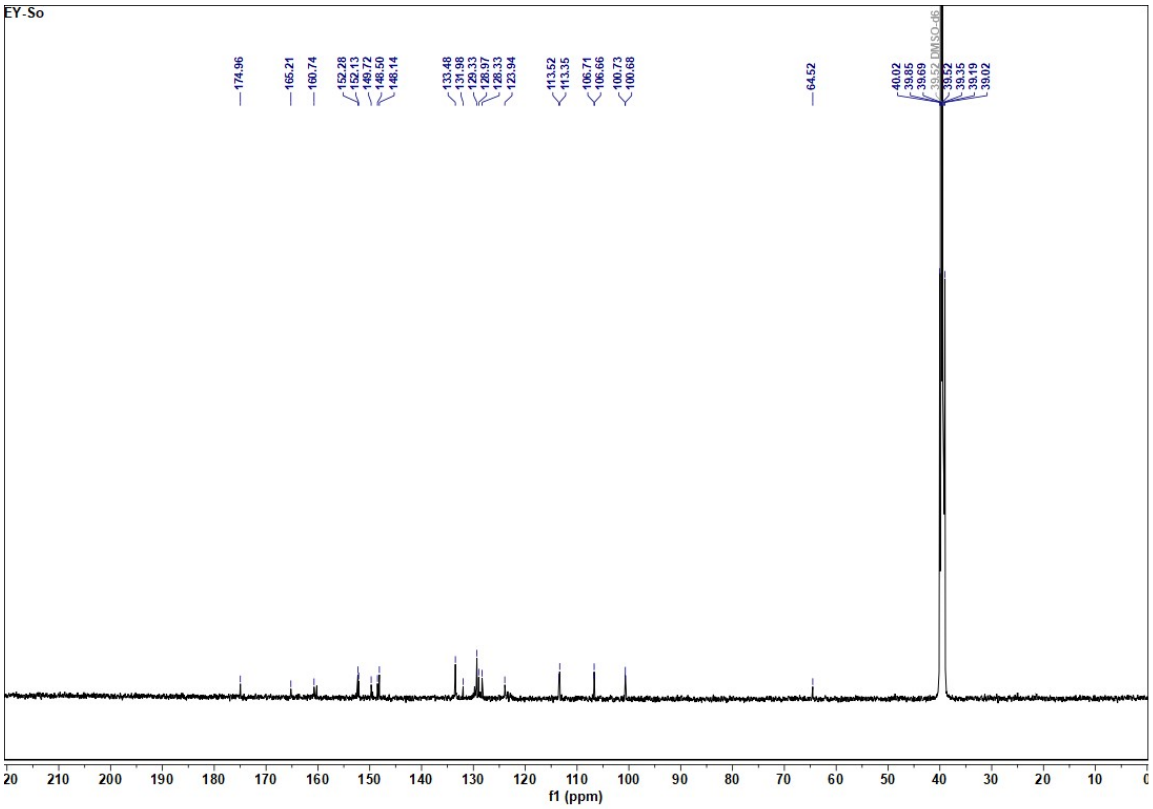

Fig. S5: $^{13}C\{^{1}H\}$ NMR spectrum of **EY-So**

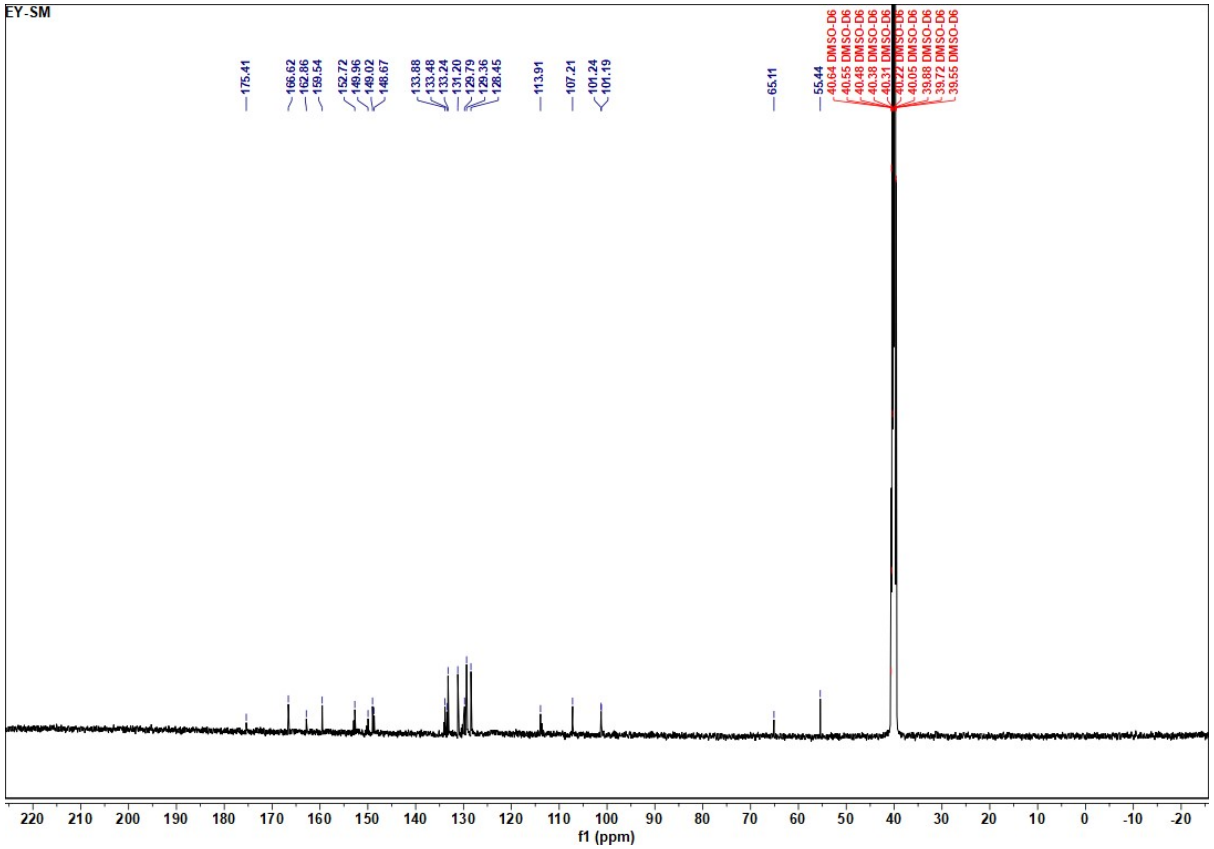

Fig. S6: $^{13}C\{^{1}H\}$ NMR spectrum of **EY-S$_M$**

Sensing Experiment

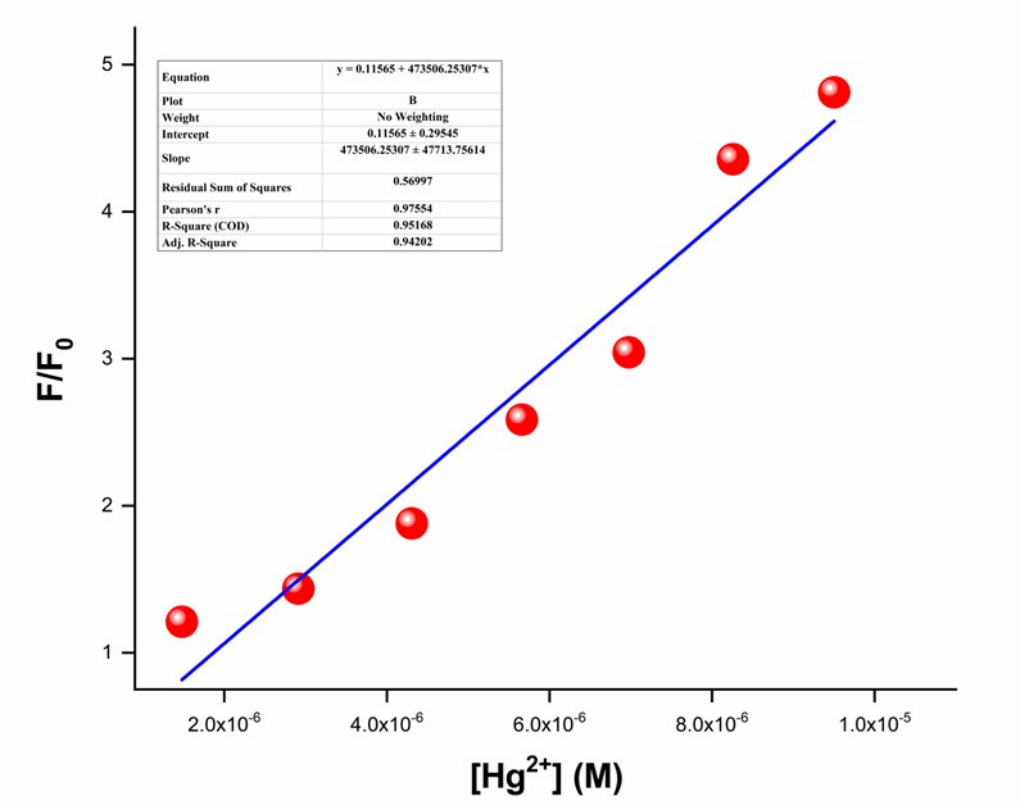

Fig. S7: Emission titration plot (Fluorescence intensity vs $[Hg^{2+}]$) of **EY-S$_O$** (10^{-5} M) and Hg^{2+} (10^{-4} M) in ethanol–water (1:1) at pH 7.2 and 25°C. (Inset: Emission titration plot till 1.5 equivalent of Hg^{2+} to **EY-S$_O$**). Slope = $8.89817\times10^{10} \pm 8.43119\times10^{9}$.

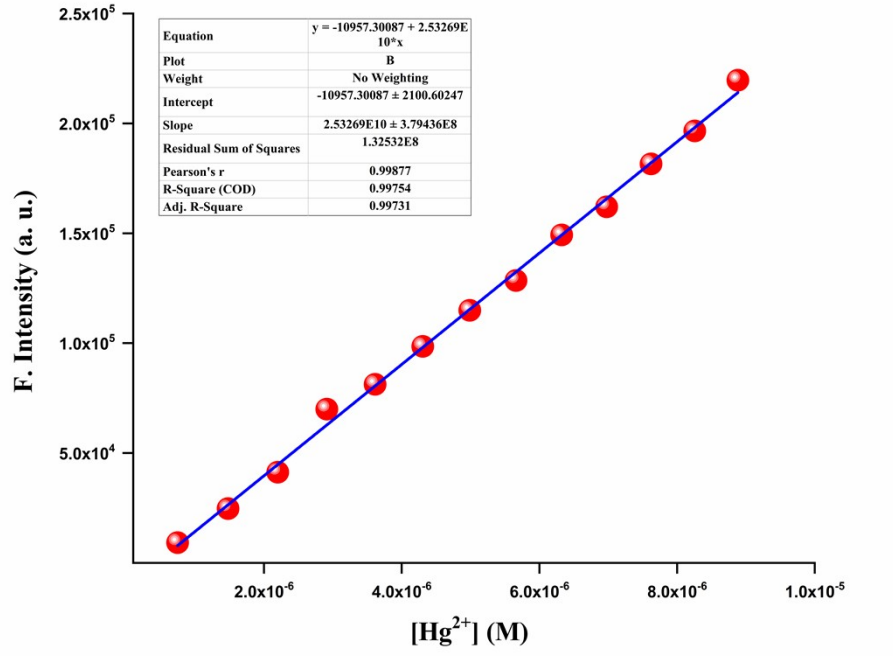

Fig. S8: Emission titration plot (Fluorescence intensity vs $[Hg^{2+}]$) of **EY-S$_M$** (10^{-5} M) and Hg^{2+} (10^{-4} M) in ethanol–water (1:1) at pH 7.2 and 25°C. (Inset: Emission titration plot till 1.5 equivalent of Hg^{2+} to **EY-S$_M$**). Slope = $2.53269\times10^{10}\pm3.79436\times10^{8}$.

Fig. S9: Plot of Relative fluorescence intensity vs. concentration of **EY-S_M**. Slope = 473506.25307 ± 47713.75614.

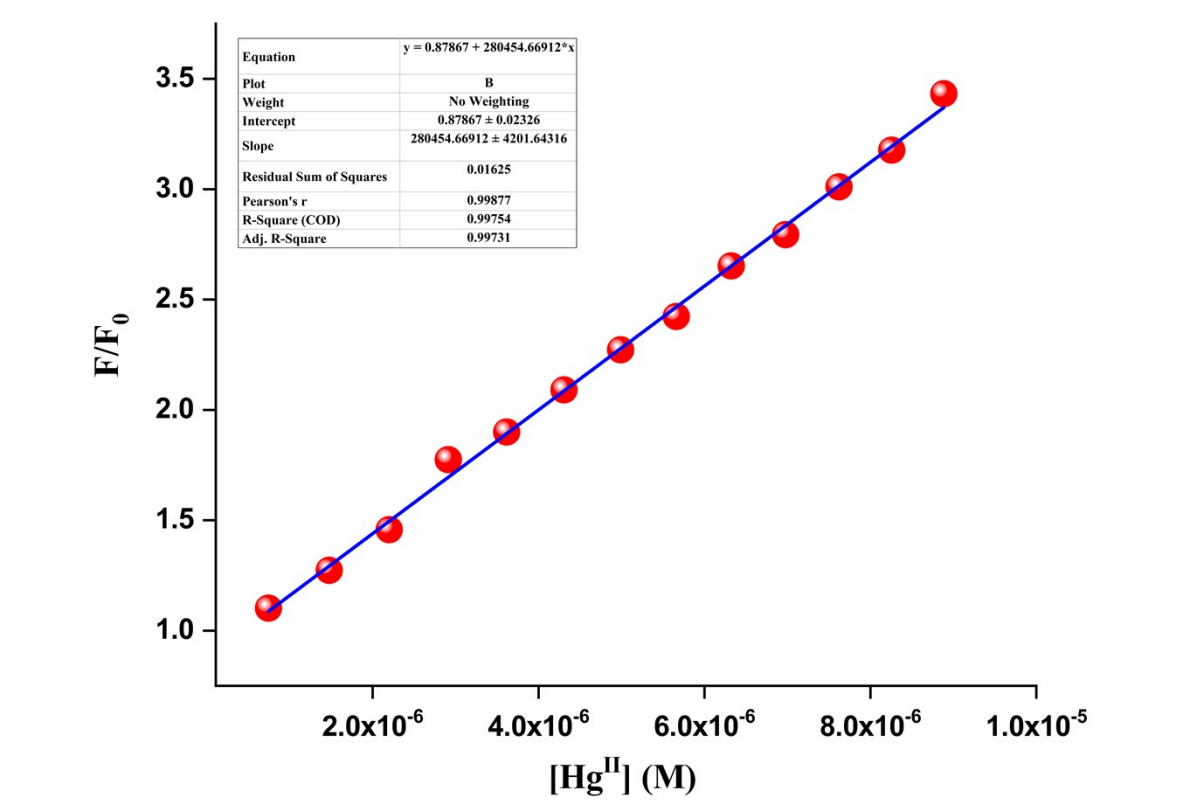

Fig. S10: Plot of Relative fluorescence intensity vs. concentration of **EY-S_M**. Slope = 280454.66912 ± 4201.64316.

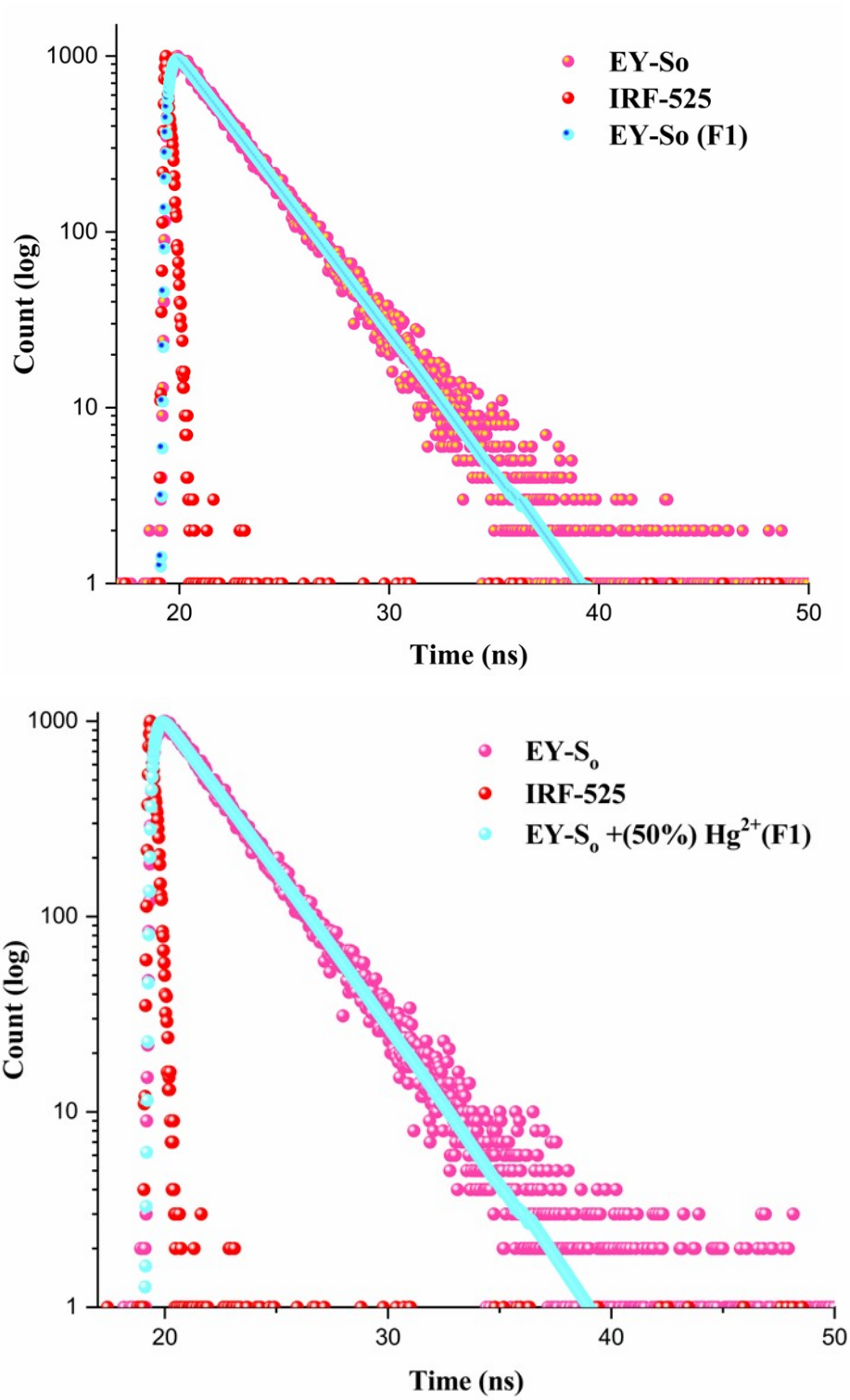

Fig S11: Lifetime data of **EY-S$_O$** (Top) and **EY-S$_O$** + 50% Hg^{2+} (Bottom)

The obtained lifetime decays are fitted with the tri-exponential functions as given in following equation, where the reduced χ^2 gives the virtue of the fitting

Finally, average lifetime of **EY-S$_O$** was calculated using the following equation:

$\langle\tau\rangle_{avg} = (B_1\tau_1^2 + B_2\tau_2^2 + B_3\tau_3^2) / (B_1\tau_1 + B_2\tau_2 + B_3\tau_3)$.

For **EY-S$_O$**,

$\langle\tau\rangle_{avg} = [\ (0.108\times0.0100^2) + (0.087\times2.7880^2) + (-0.001\times6.2758^2)] / [\ (0.108\times0.0100) + (0.087\times2.7880) + (-0.001\times6.2758)\ ]$

$=2.69$ ns

Similarly, for **EY-S_O + 25% Hg^{2+},**

$\langle\tau\rangle_{avg} = 2.730$ ns.

for **EY-S_O + 50% Hg^{2+},**

$\langle\tau\rangle_{avg} = 2.753$ ns.

for **EY-S_O + 75% Hg^{2+},**

$\langle\tau\rangle_{avg} = 2.756$ ns.

for **EY-S_O + 100% Hg^{2+},**

$\langle\tau\rangle_{avg} = 2.76$ ns.

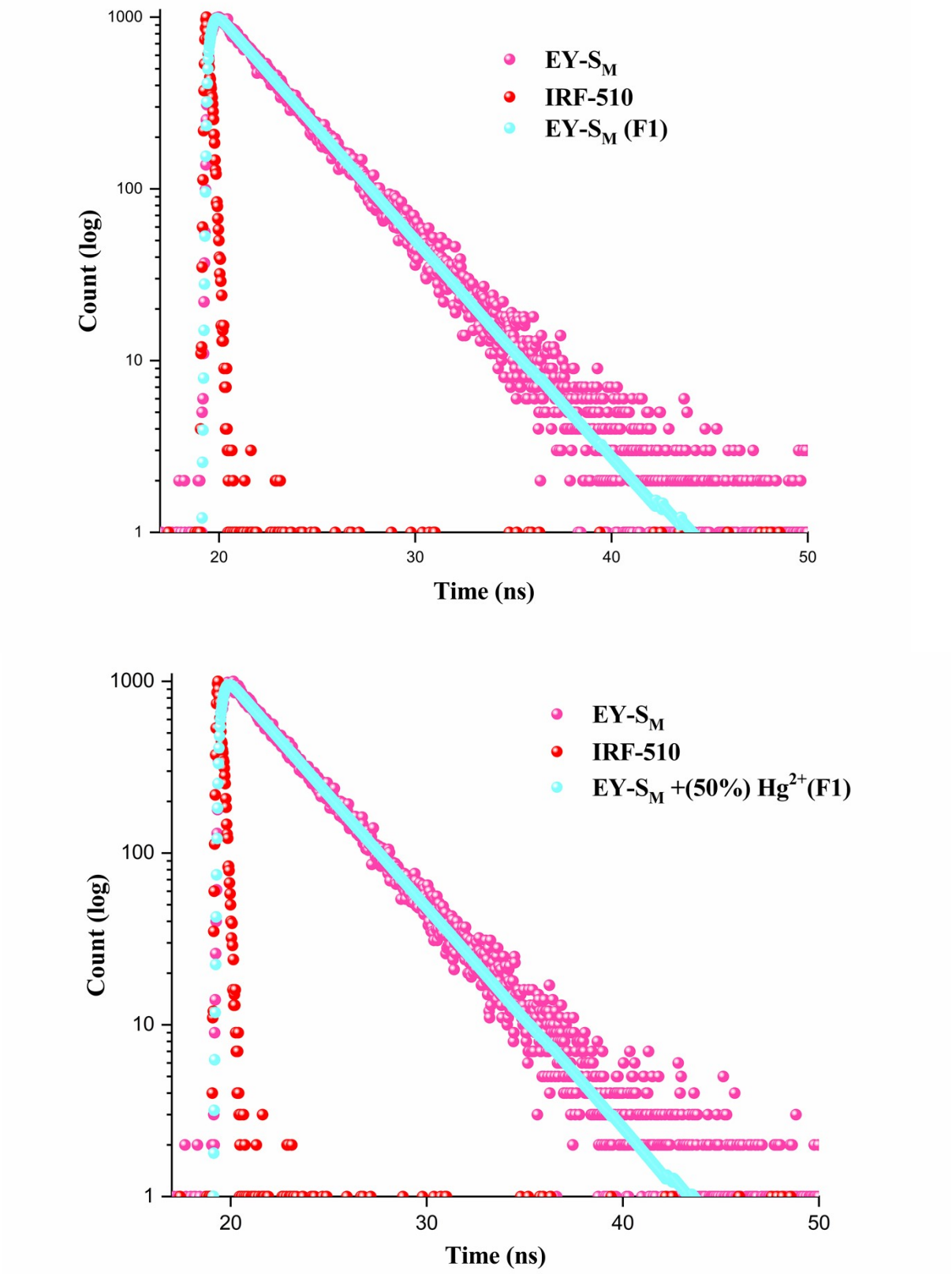

Fig S12: Lifetime data of **EY-S$_M$** (Top) **EY-S$_M$** + 50% Hg^{2+} (Bottom)

The obtained lifetime decays are fitted with the tri-exponential functions as given in following equation, where the reduced χ^2 gives the virtue of the fitting

Finally, average lifetime of **EY-S_M** was calculated using the following equation:

$\langle\tau\rangle_{avg} = (B_1\tau_1^2 + B_2\tau_2^2 + B_3\tau_3^2) / (B_1\tau_1 + B_2\tau_2 + B_3\tau_3)$.

$\langle\tau\rangle_{avg} = [(0.279\times0.0100^2) + (0.083\times3.3189^2) + (0.000\times20.000^2)] / [(0.279\times0.0100) + (0.083\times3.3189) + (0.000\times20)]$

$=3.28$ ns

Similarly, for **EY-S_M + 25% Hg^{2+},**

$\langle\tau\rangle_{avg} = 3.29$ns.

for **EY-S_M + 50% Hg^{2+},**

$\langle\tau\rangle_{avg} = 3.31$ ns.

for **EY-S_M + 75% Hg^{2+},**

$\langle\tau\rangle_{avg} = 3.330$ ns.

for **EY-S_M + 100% Hg^{2+},**

$\langle\tau\rangle_{avg} = 3.350$ ns.

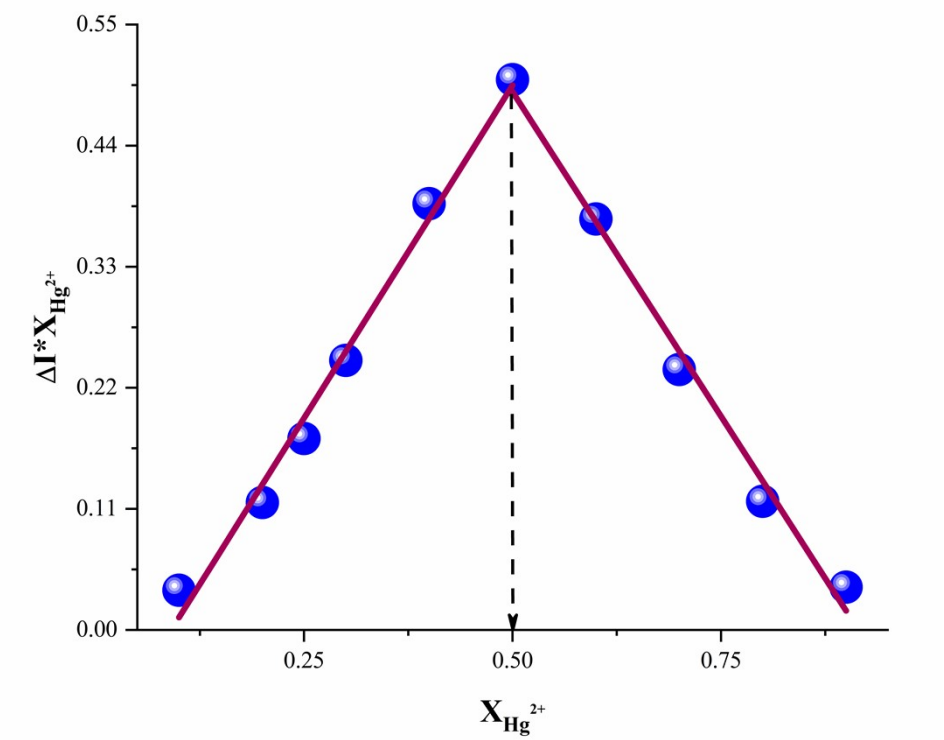

Fig. S13: Job's plot by fluorescence method. Concentration of both **EY-S$_O$** and Hg^{2+} were 10^{-6} M, solvent mixture was ethanol-water (1:1, v/v) and pH was maintained at 7.2 by Tris–HCl buffer at 25°C.

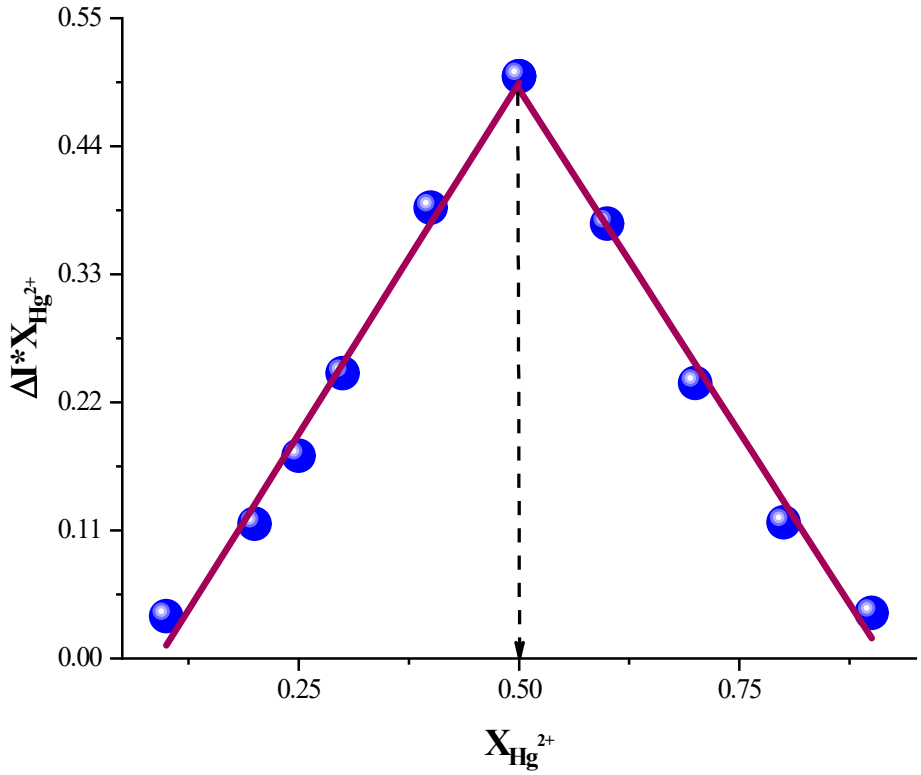

Fig. S14: Job's plot by fluorescence method. Concentration of both **EY-S$_M$** and Hg^{2+} were 10^{-6} M, solvent mixture was ethanol-water (1:1, v/v) and pH was maintained at 7.2 by Tris–HCl buffer at 25°C.

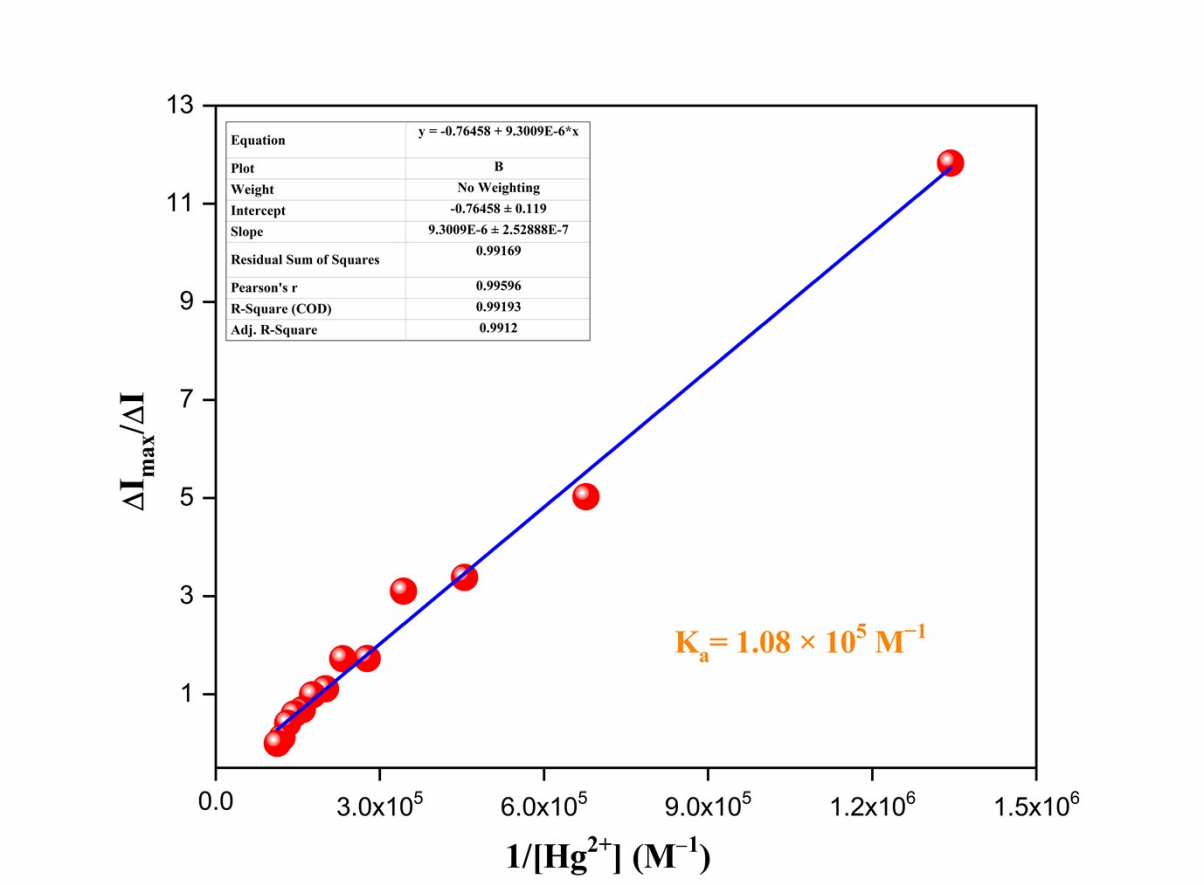

Fig. S15: B-H plot **EY-S_M**

Table. S1: Limit of detection and limit of quantification calculation of **EY-S_O**

Calculation of standard deviation of Fluorescence intensity of **EY-S_O**

Reading of EY-S_O at Wavelength = 534	**F. I.**
Reading 1	166205.66
Reading 2	165979.94
Reading 3	165867.08
Reading 4	166092.80
Reading 5	166318.52

Standard deviation (σ) = 178.36

Slope (K) of fluorescence spectrum (Fluorescence intensity vs $[Hg^{2+}]$) = $8.89817 \times 10^{10} \pm 8.43119 \times 10^{9}$.

For fluorescence method, $\sigma/K = 2.004 \times 10^{-9}$.

LOD = 6.012×10^{-9} M.

LOQ = 2.004×10^{-8} M.

Table. S2: Limit of detection and limit of quantification calculation of **EY-S_M**

Calculation of standard deviation of Fluorescence intensity of **EY-S_M**

Reading of EY-S_M at Wavelength = 551	**F. I.**
Reading 1	90243.23
Reading 2	90274.88
Reading 3	90306.53
Reading 4	90338.18
Reading 5	90369.83

Standard deviation (σ) = 50.03

Slope (K) of fluorescence spectrum (Fluorescence intensity vs $[Hg^{2+}]$) = $2.53269\times10^{10} \pm 3.79436\times10^{8}$.

For fluorescence method, $\sigma/K = 1.976 \times 10^{-9}$.

LOD = 5.929×10^{-9} M.

LOQ = 1.976×10^{-8} M.

Table S3: LOD of different sensors in mercury sensing

Sl. No.	LOD	Solvent system	Reference
1	3.6 nM	CH_3CN/H_2O (1/1, v/v)	[2]
2	3.3 nM	HEPES buffer- ethanol (pH 8.0, 3:2)	[3]
3	15.7 nM	MeOH–HEPES (0.4 M, pH 7.0, 6:4)	[4]
4	20 nM	1,4-Dioxane–PBS (20 mM, pH 7.0, 0.5:99.5)	[5]
5	26.8 nM	(citric acid / M Na_2HPO_4) prepared in deionized water (0.1 M / 0.2 ; pH 7.0)	[6]
6	0.22 μM	CH3CN–HEPES (10 mM, pH 7.4, 4:1)	[7]
7	86 nM	H_2O (With 0.01% DMSO) (pH 6 to 9, 1:1)	[8]
8	1.2 ppb	MeOH/H2O (3:2 v/v)	[9]
9	0.63 μM	PBS/DMF (pH = 7.4, containing 10% DMF)	[10]
10	16.8 nM	Na2HPO4-citric acid buffer	[11]
11	6.01 nM	Ethanol–tris buffer (1:1, pH 7.2) (EY-S_O)	Present work
12	5.92nM	Ethanol–tris buffer (1:1, pH 7.2) (EY-S_M)	Present work

Table S4: selectivity and interference Data of **EY-S_O** with other metals (% Intensity). Data represented as mean ± SD (n = 3).

Metal	% Intensity (mean ± SD)		
	EY-S_O	**(500 mol%) Metal**	**(100 mol%) Hg^{2+}**
K(I)	14.54 ± 0.43	15.3018 ± 0.51	100 ± 3.59
Cu(I)	14.54 ± 0.43	14.93018 ± 0.53	100 ± 4.88
Ag(I)	14.54 ± 0.43	14.3018 ± 0.46	100 ± 3.99
Fe(II)	14.54 ± 0.43	15.3018 ± 0.36	100 ± 3.46
Mn(II)	14.54 ± 0.43	15.3018 ± 0.39	100 ± 4.52
Co(II)	14.54 ± 0.43	15.9018 ± 0.44	100 ± 4.21
Ni(II)	14.54 ± 0.43	15.3018 ± 0.51	100 ± 3.85
Cu(II)	14.54 ± 0.43	15.3018 ± 0.52	100 ± 4.21
Zn(II)	14.54 ± 0.43	15.3018 ± 0.48	100 ± 4.17
Pb(II)	14.54 ± 0.43	15.3018 ± 0.41	100 ± 4.26
Al(III)	14.54 ± 0.43	15.3018 ± 0.44	100 ± 4.21
Cr(III)	14.54 ± 0.43	15.3018 ± 0.54	100 ± 3.93
Fe(III)	14.54 ± 0.43	15.3018 ± 0.36	100 ± 4.12

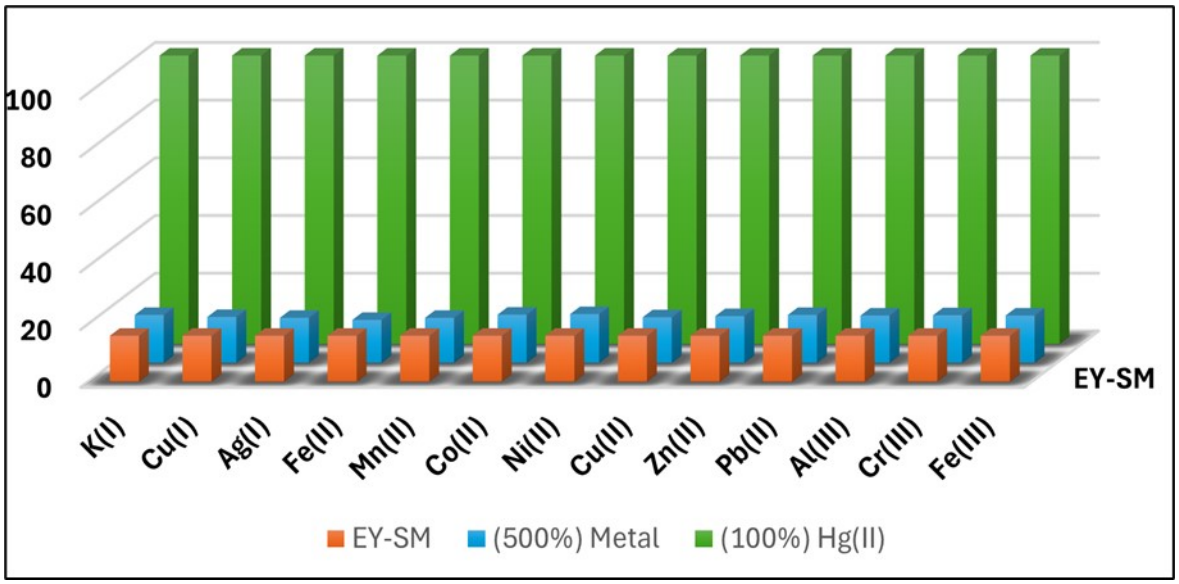

Fig. S16: Interaction of **EY-S_M** with other metals and effect of interference of other metal.

Table. S5: selectivity and interference Data of **EY-S_M** with other metals (% Intensity). Data represented as mean ± SD (n = 3).

Metal	% Intensity (mean ± SD)		
	EY-S_M	**(500 mol%) Metal**	**(100 mol%) Hg^{2+}**

K(I)	15.91 ± 0.31	16.6 ± 0.52	100 ± 4.21
Cu(I)	15.91 ± 0.31	15.9 ± 0.47	100 ± 4.47
Ag(I)	15.91 ± 0.31	15.6 ± 0.48	100 ± 3.91
Fe(II)	15.91 ± 0.31	14.9 ± 0.31	100 ± 4.09
Mn(II)	15.91 ± 0.31	15.6± 0.38	100 ± 4.21
Co(II)	15.91 ± 0.31	16.7± 0.41	100 ± 4.11
Ni(II)	15.91 ± 0.31	16.9 ± 0.44	100 ± 4.36
Cu(II)	15.91 ± 0.31	15.8 ± 0.48	100 ± 3.46
Zn(II)	15.91 ± 0.31	16.2 ± 0.52	100 ± 4.25
Pb(II)	15.91 ± 0.31	16.6 ± 0.39	100 ± 4.31
Al(III)	15.91 ± 0.31	16.4 ± 0.33	100 ± 4.02
Cr(III)	15.91 ± 0.31	16.5 ± 0.37	100 ± 4.62
Fe(III)	15.91 ± 0.31	16.4 ± 0.38	100 ± 3.11

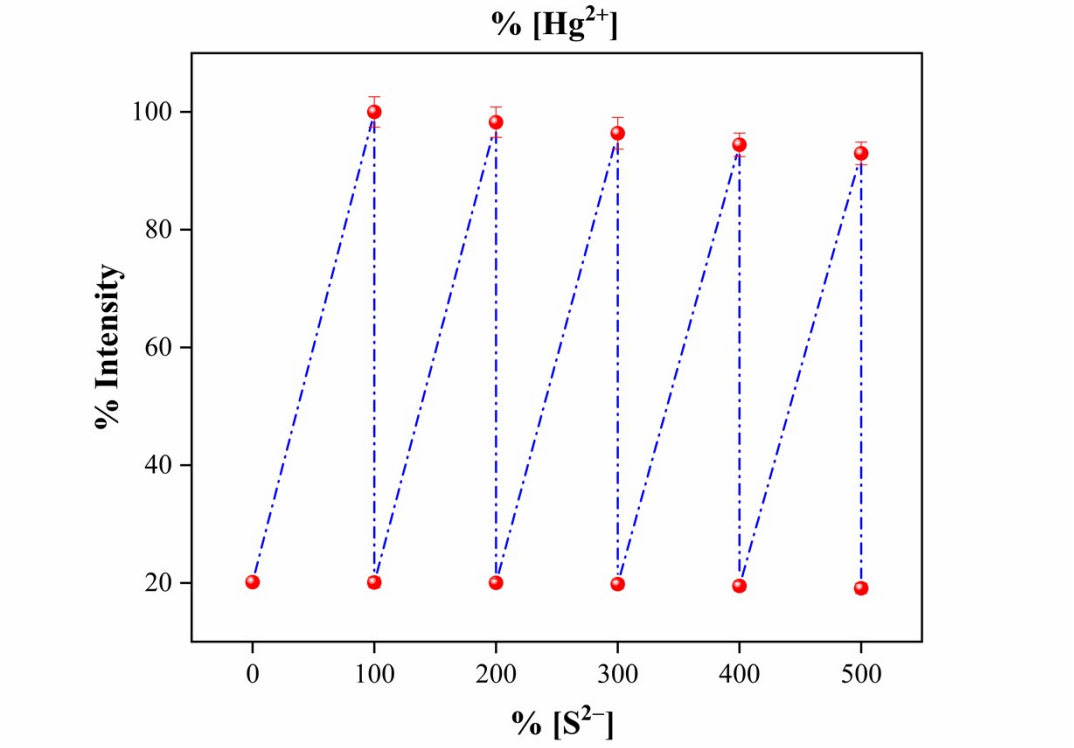

Fig. S17: Recyclability of **EY-S_O** using sulphide ion (S^{2-}).

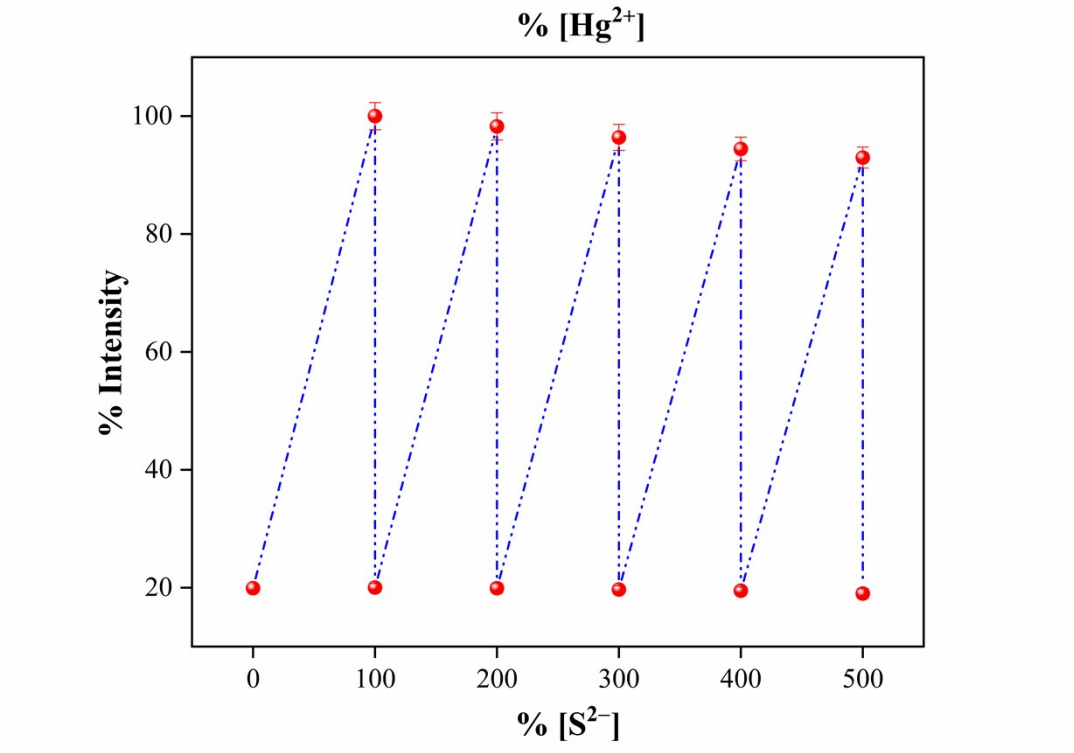

Fig. S18: Recyclability of **EY-S_M** using sulphide ion (S^{2-}).

IR

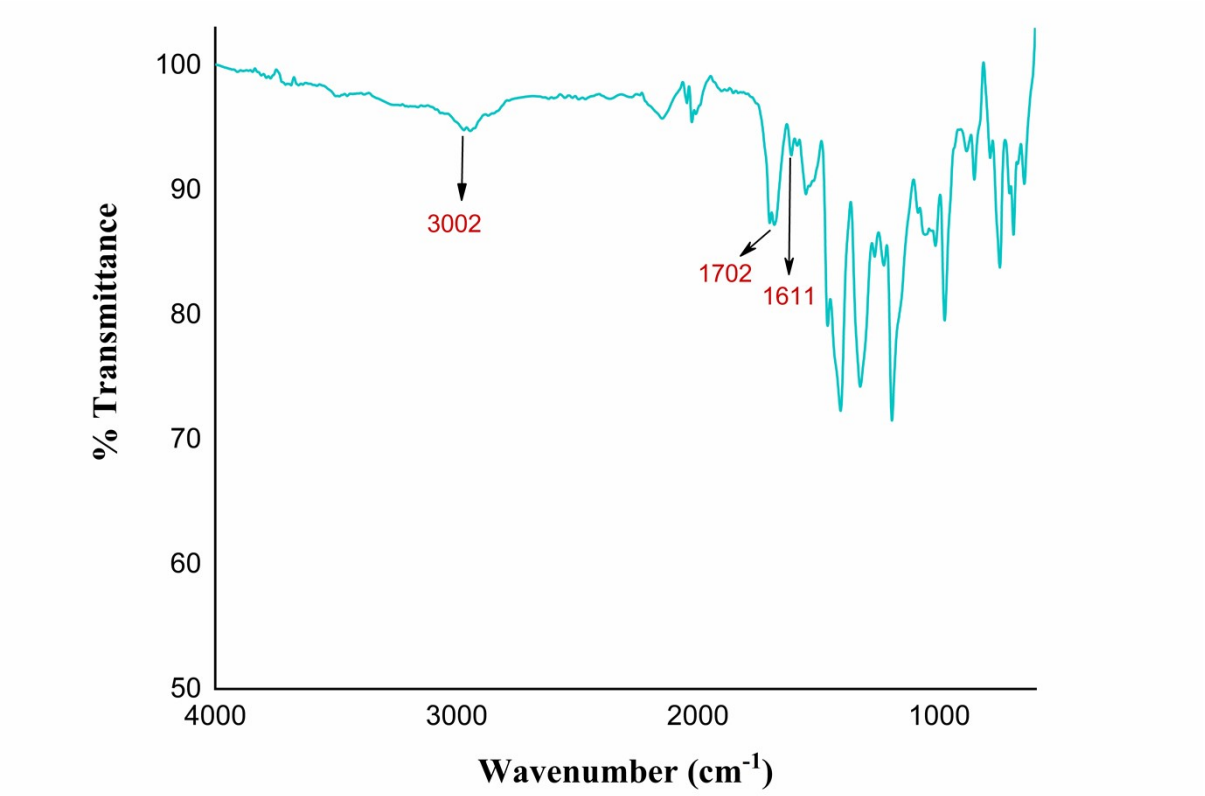

Fig. S19: IR spectrum of **EY-M_O.**

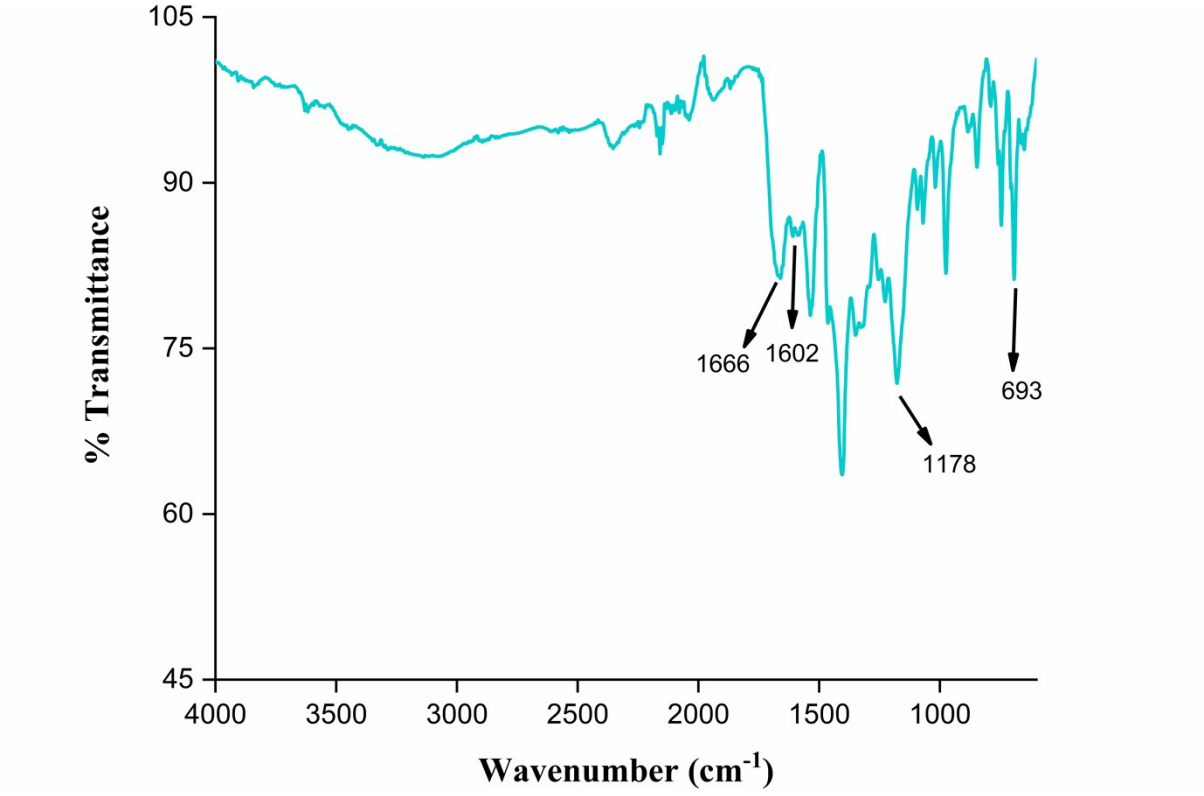

Fig. S20: IR spectrum of **EY-M_M.**

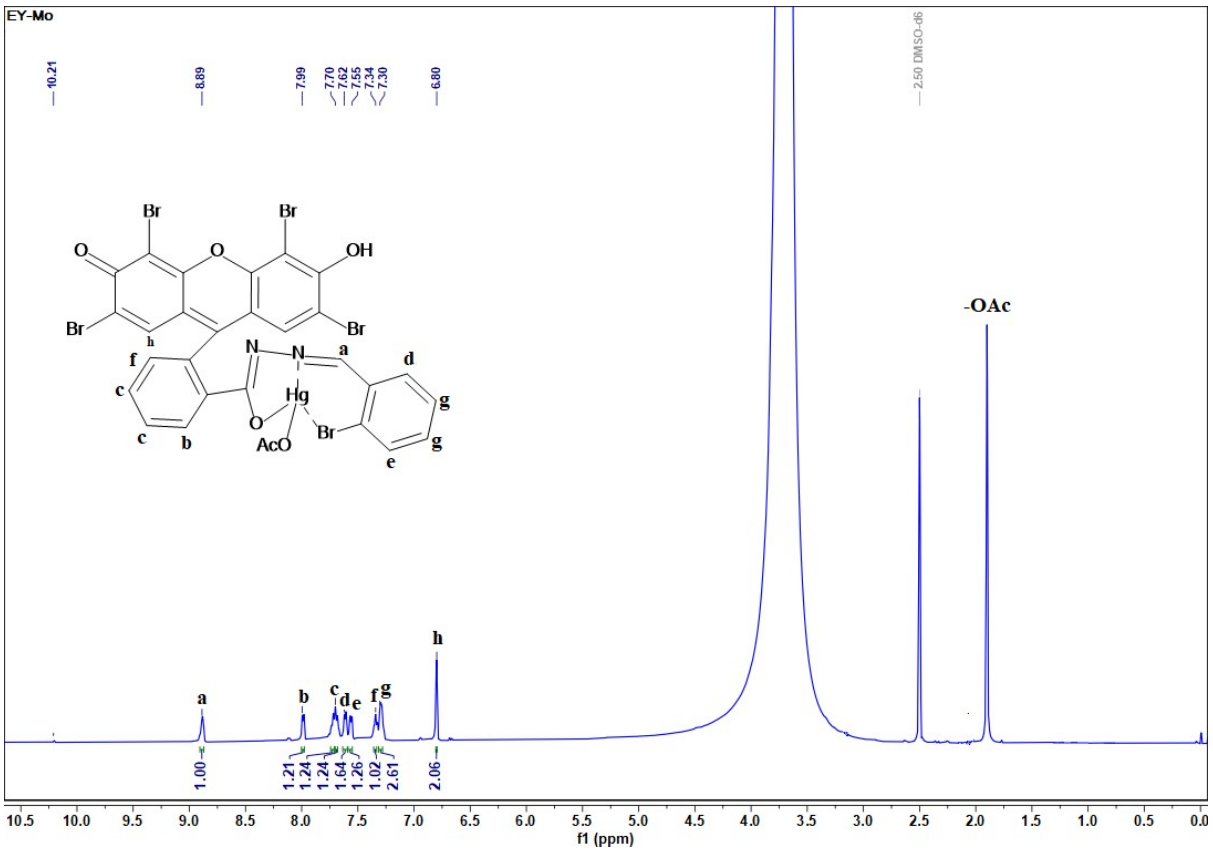

^{1}H NMR

Fig. S21: ^{1}H NMR spectrum of **EY-M$_{O}$**.

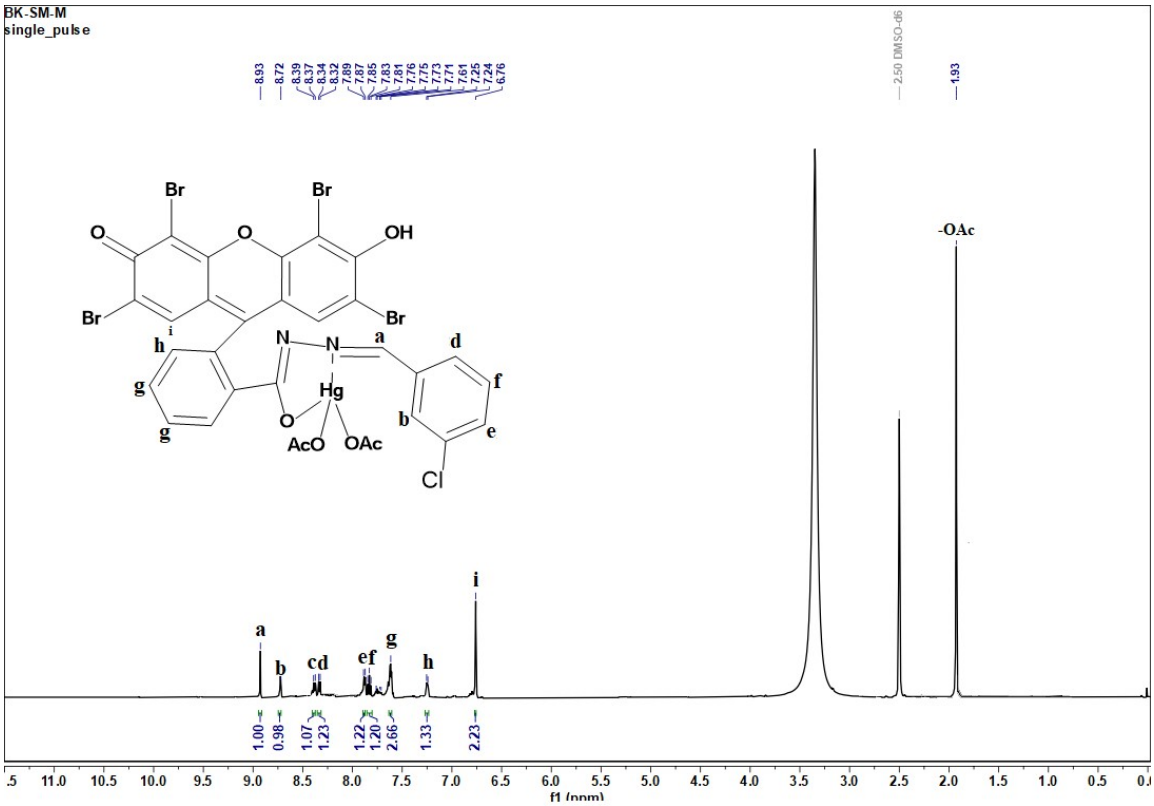

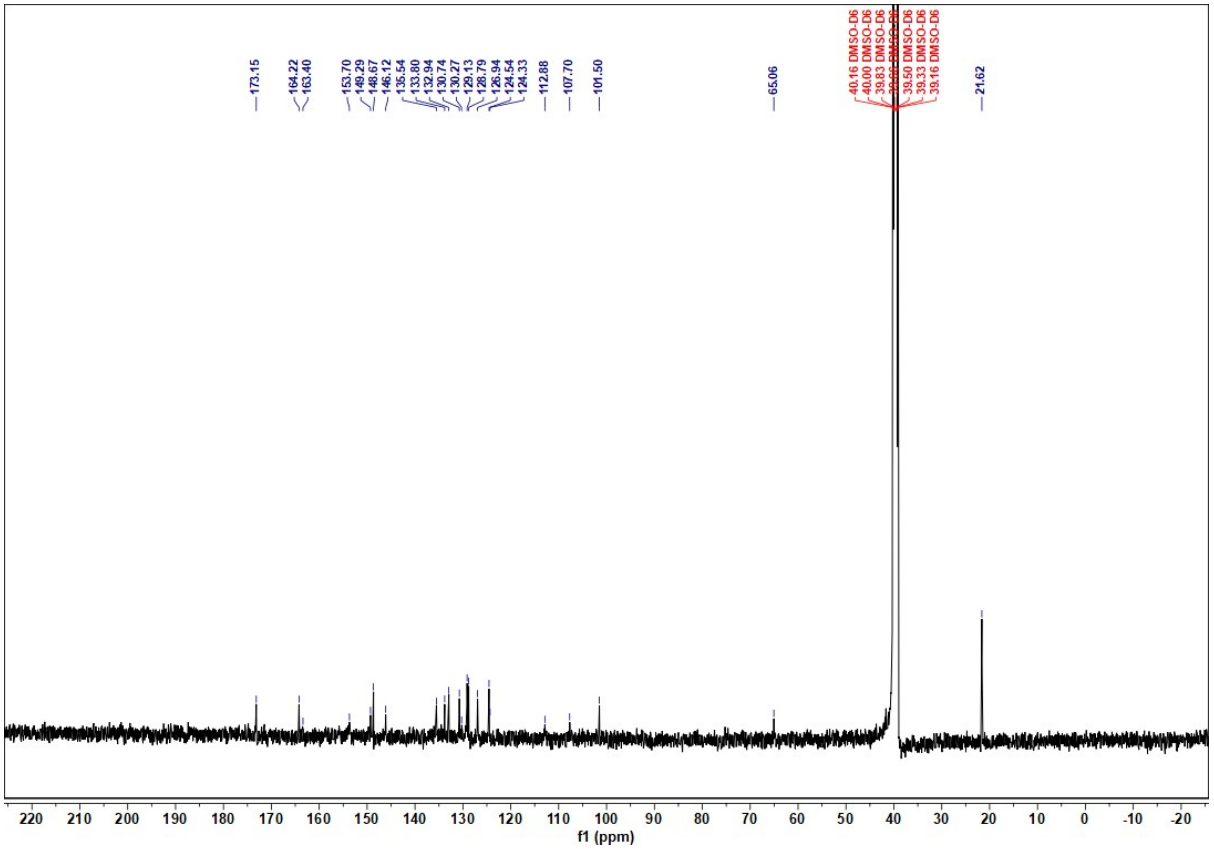

Fig. S22: ^{1}H NMR spectrum of **EY-M$_{M}$**.

^{13}C{^{1}H} NMR

Fig. S23: ^{13}C{^{1}H} NMR spectrum of **EY-Mo**

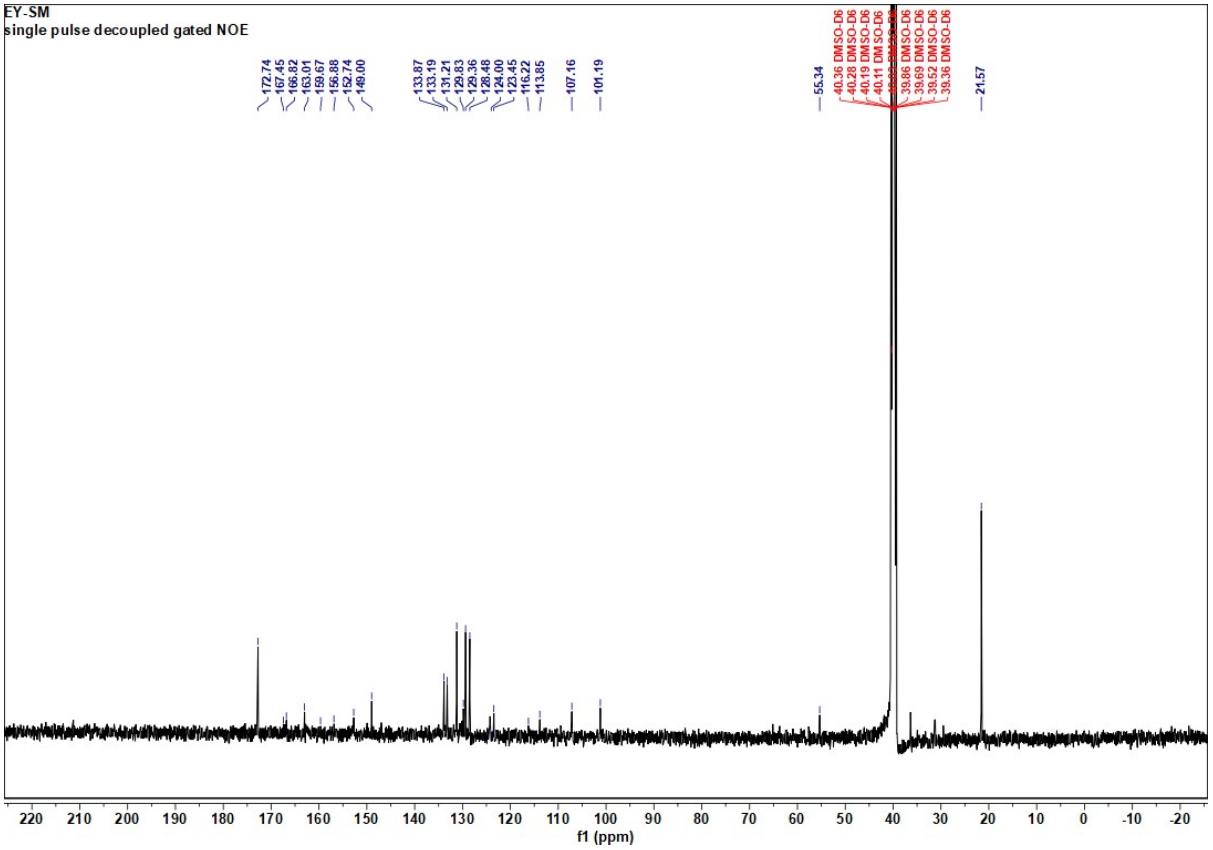

Fig. S24: $^{13}C\{^{1}H\}$ NMR spectrum of **EY-M$_M$**

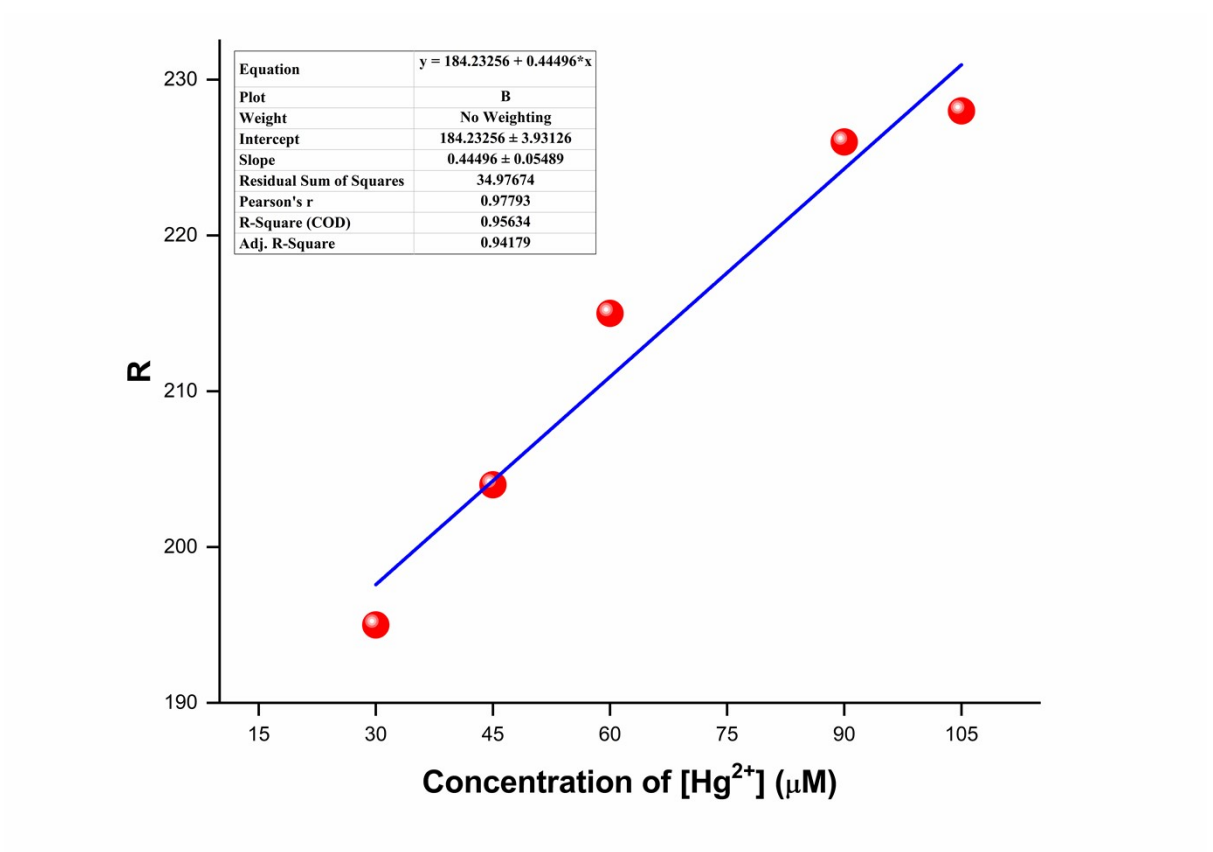

Fig S25: Normalized R vs Hg^{2+} of **EY-S$_o$**

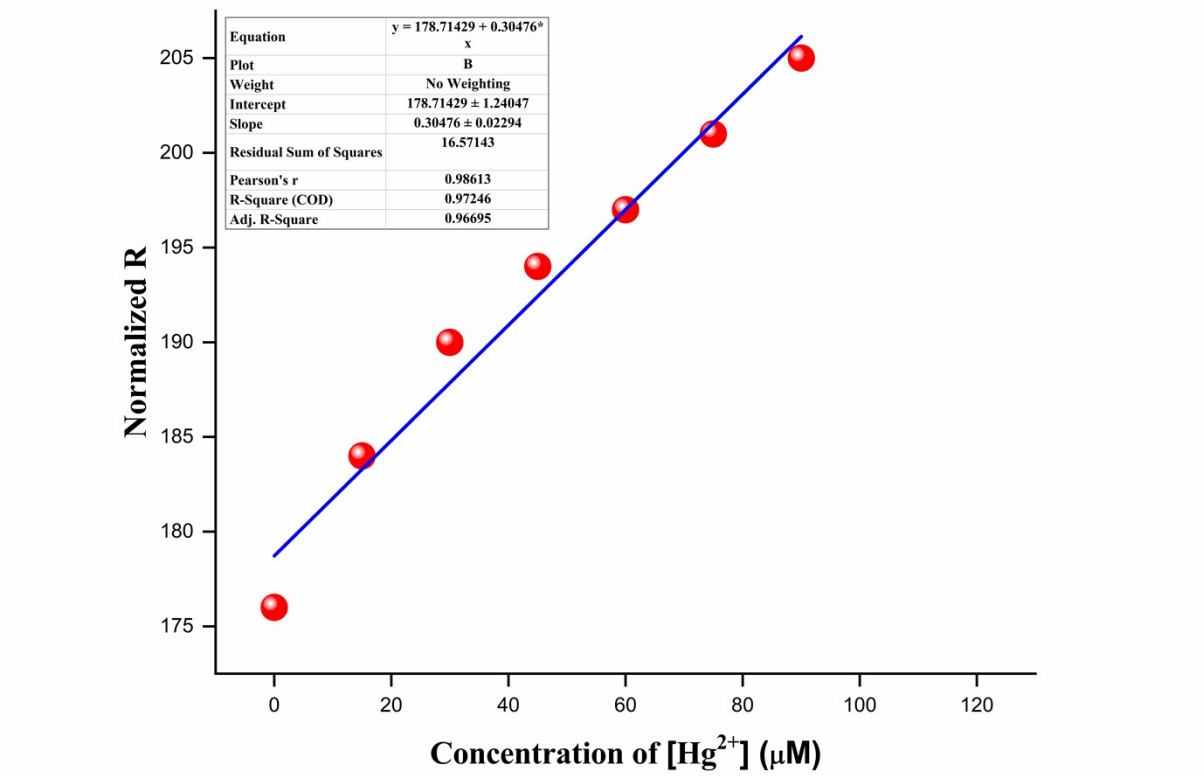

Fig S26: Normalized R vs Hg^{2+} of **EY-S_M**

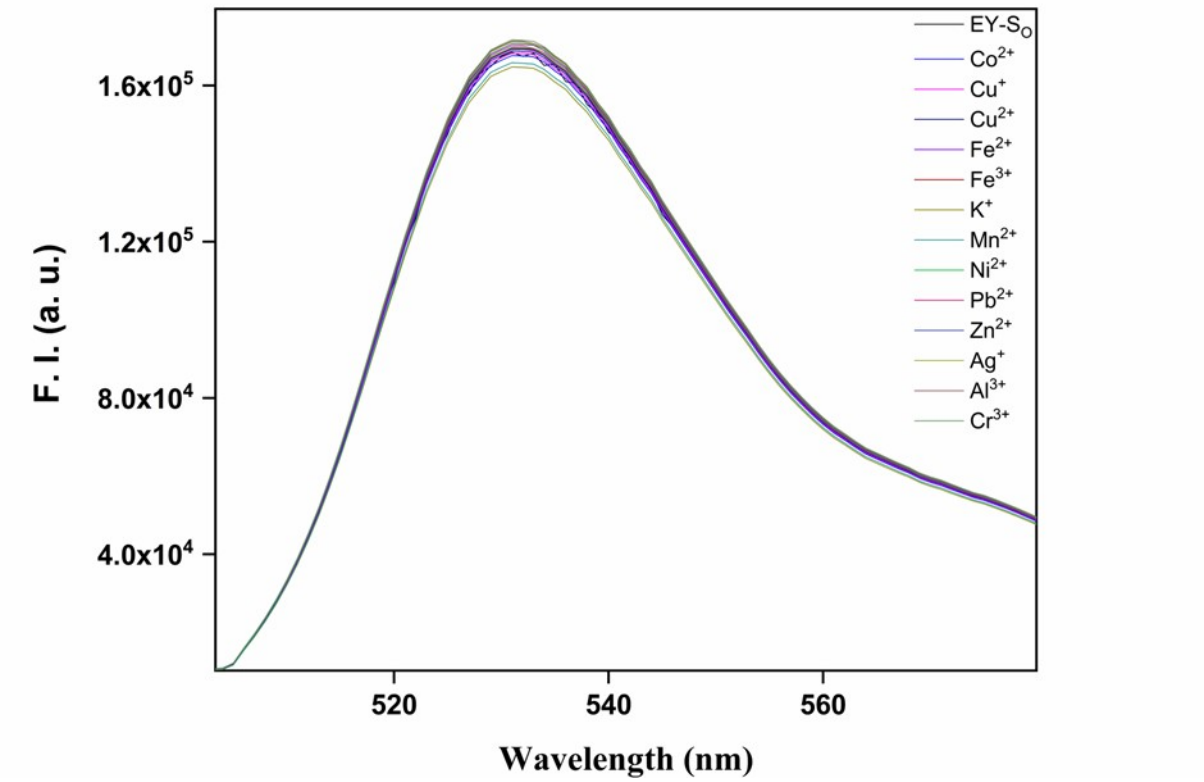

Fig S27: Fluorescence spectra of **EY-S_O** (10^{-5} M) in the presence of different metal ions (5 equiv.).

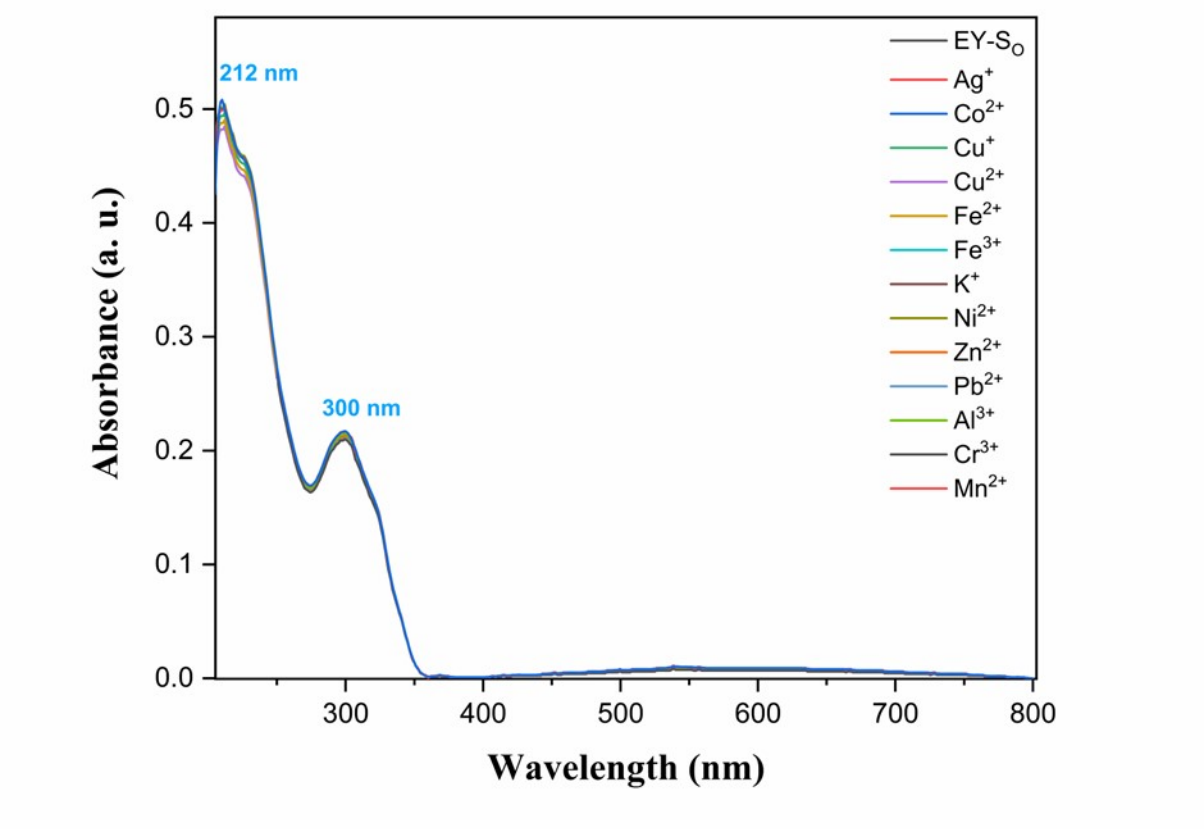

Fig S28: UV-vis absorption spectra of **EY-S$_O$** (10^{-5} M) in the presence of different metal ions (5 equiv.)

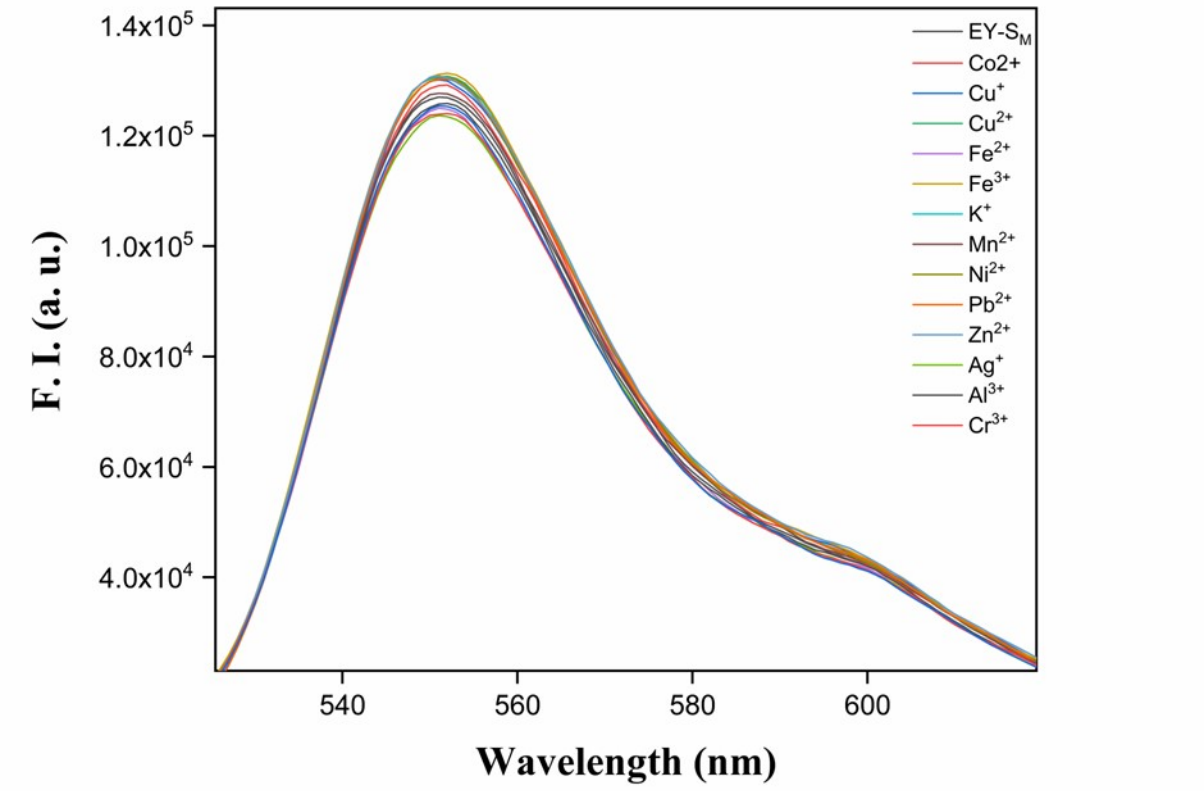

Fig.S29: Fluorescence spectra of **EY-S$_M$** (10^{-5} M) in the presence of different metal ions (5 equiv.)**.**

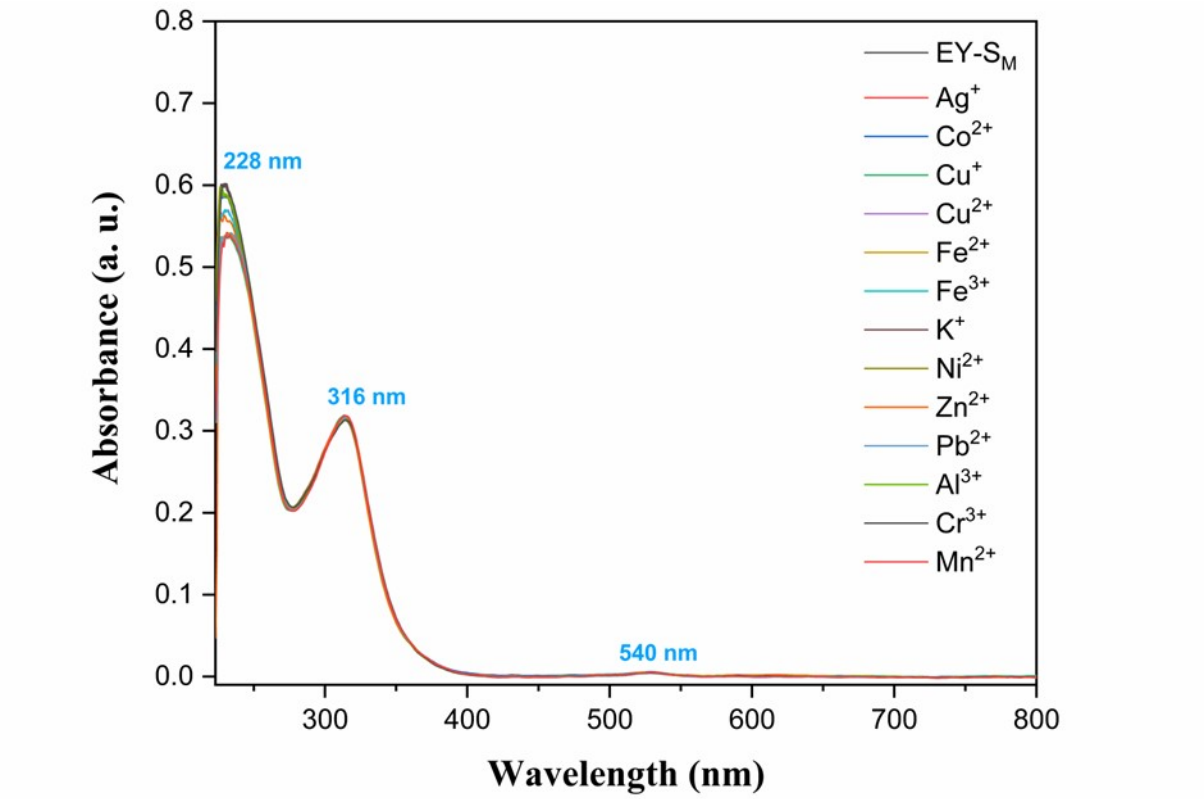

Fig S30: UV-vis absorption spectra of **EY-S$_M$** (10^{-5} M) in the presence of different metal ions (5 equiv.).

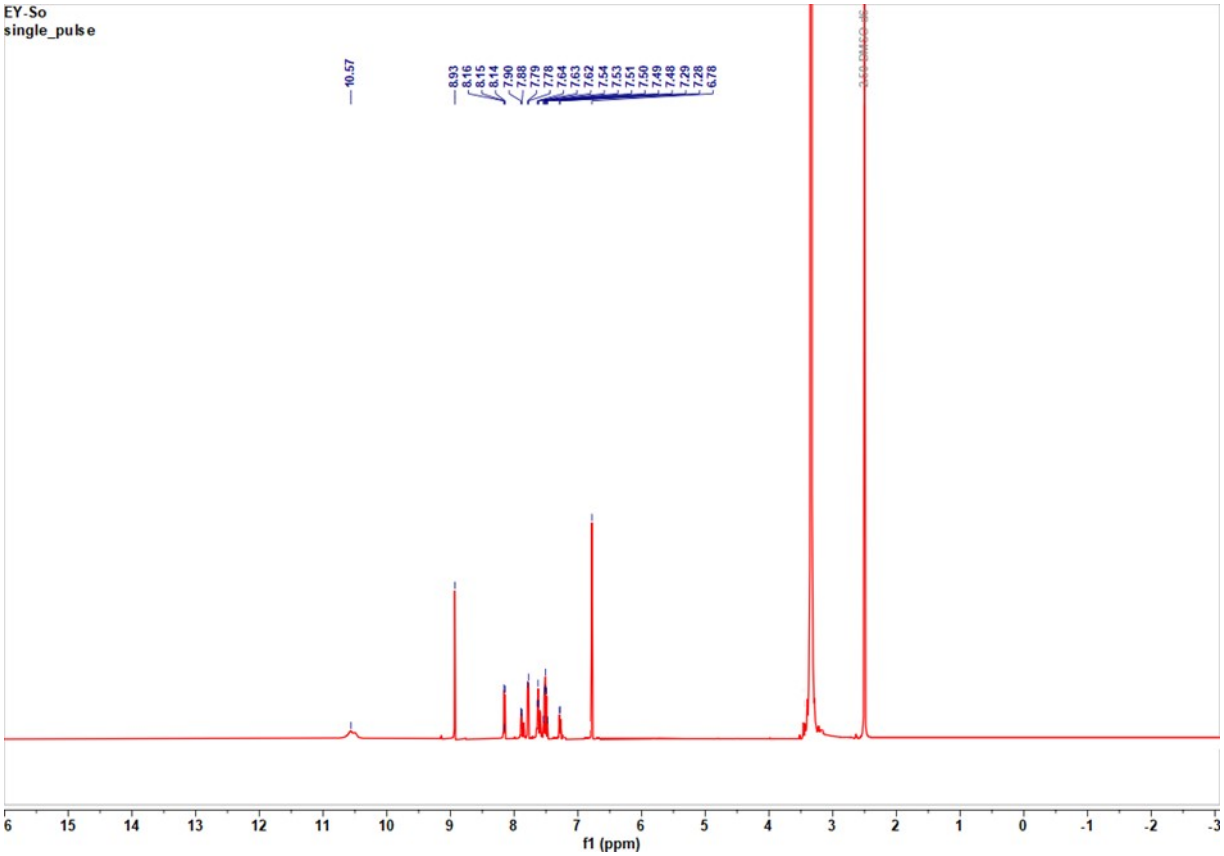

Fig. S31: ^{1}H NMR of **EY-S$_O$** + 0 equiv. Hg^{2+}.

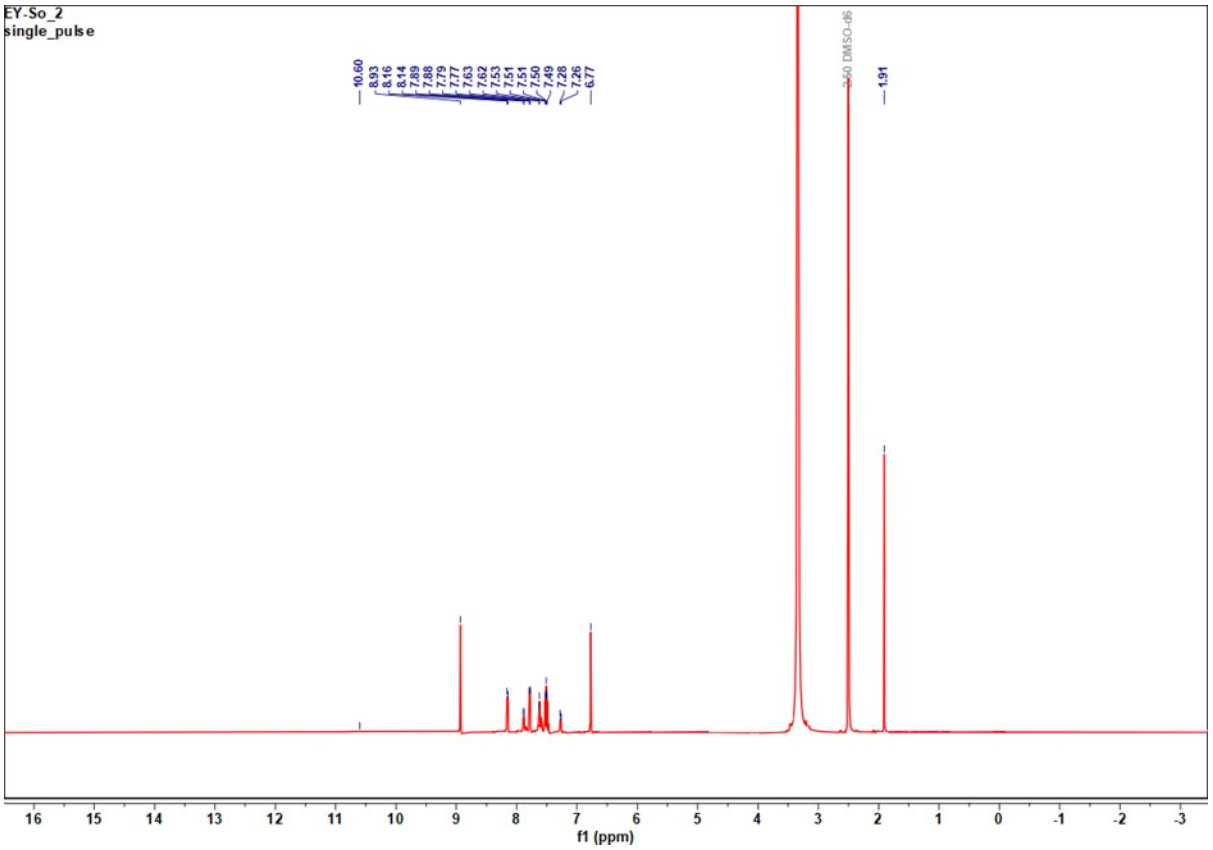

Fig. S32: ^{1}H NMR of **EY-S$_O$** + 0.2 equiv. Hg^{2+}

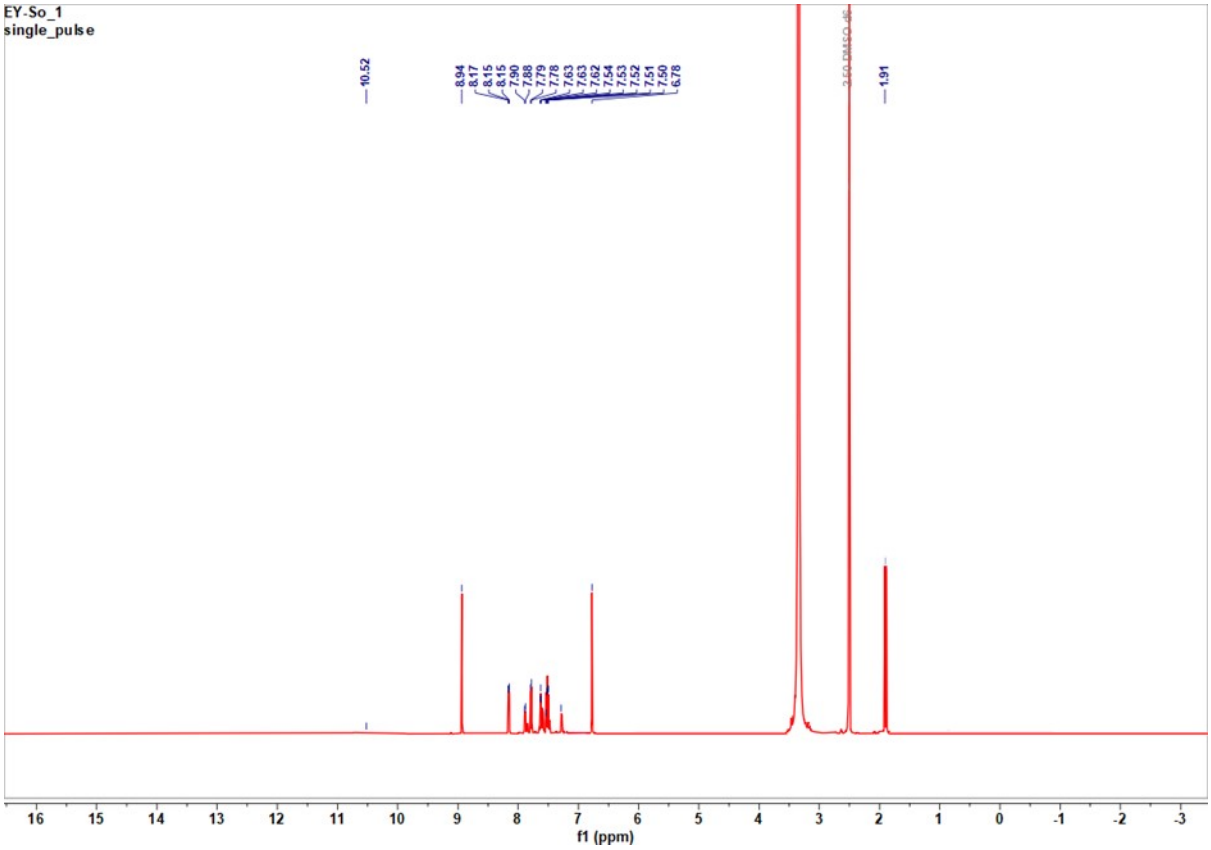

Fig. S33: ^{1}H NMR of **EY-S$_O$** + 0.4 equiv. Hg^{2+}.

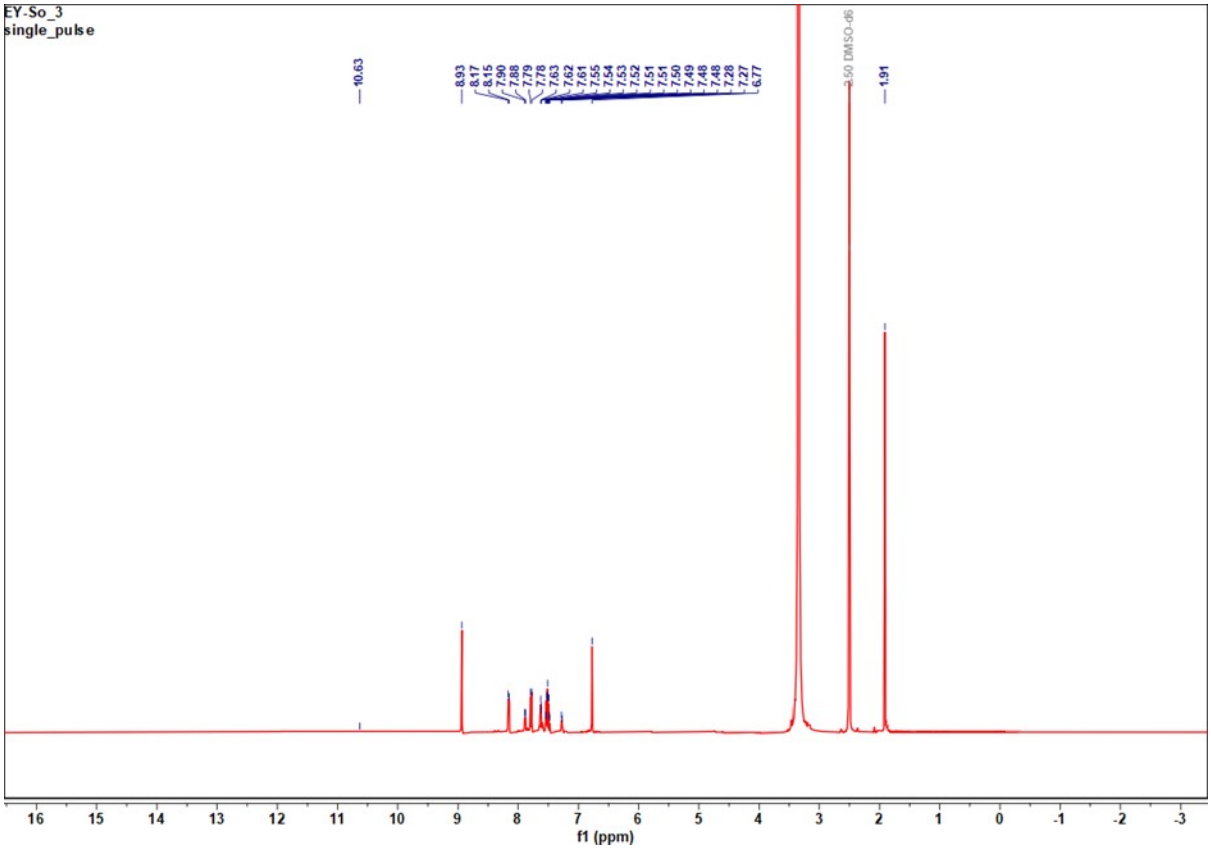

Fig. S34: ^{1}H NMR of **EY-S$_O$** + 0.6 equiv. Hg^{2+}.

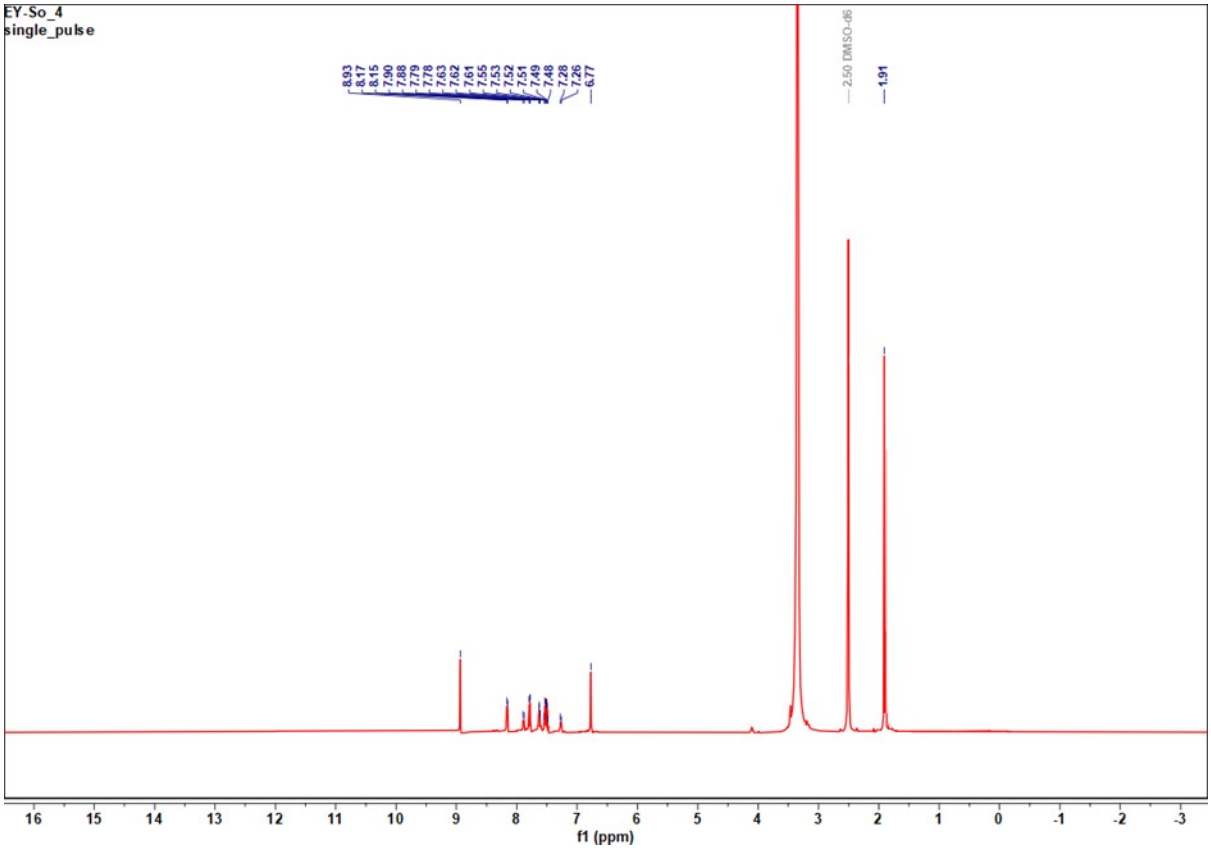

Fig. S35: ^{1}H NMR of **EY-S$_O$** + 0.8 equiv. Hg^{2+}.

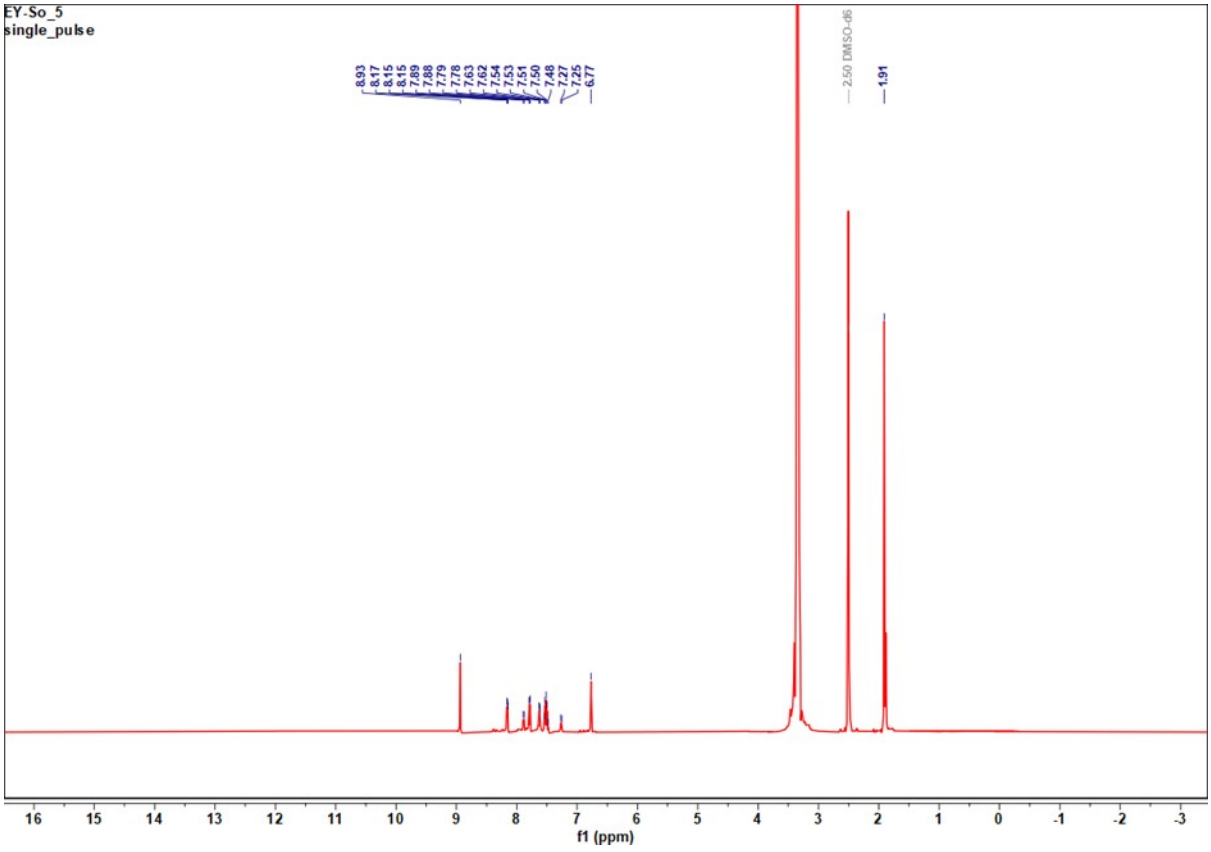

Fig. S36: ^{1}H NMR of **EY-S$_O$** + 1 equiv. Hg^{2+} (**EY-M$_O$**).

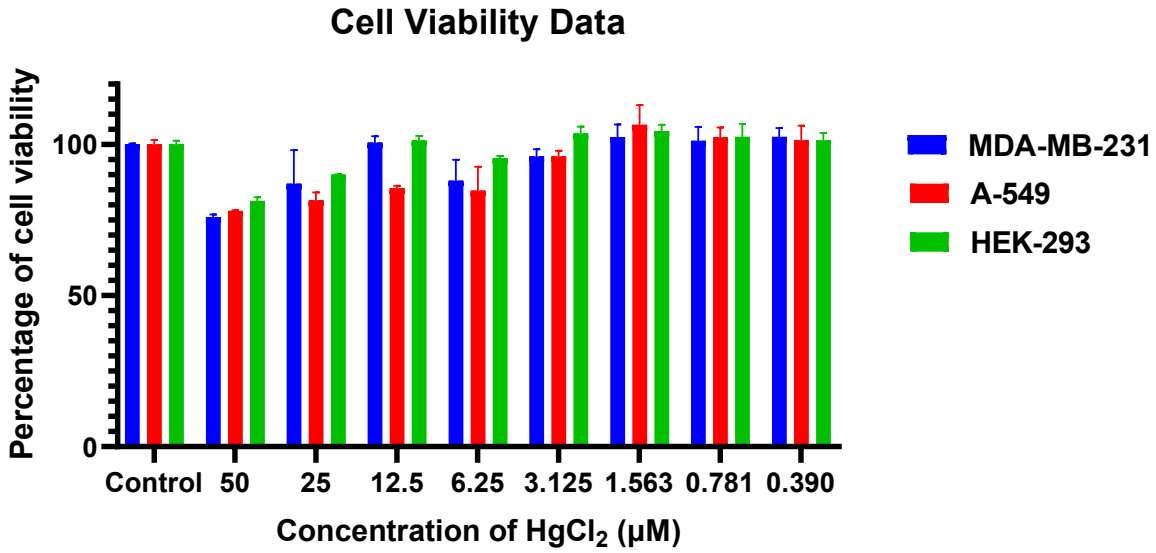

Fig. S37: Cytotoxicity data of $HgCl_2$ obtained by the MTT assay for 48 hours in MDA-MB-231, A-549 and HEK-293 cell lines. In this study the cultured cells were treated with the $HgCl_2$ in the concentration range of 0.39 to 50 µM (n=2) for 48 h. The graphs were plotted using the GraphPad Prism 8.0.1.

9: References

[1] Chakraborty, A., Rajana, V. K., Saritha, C., Srivastava, A., Mandal, D., Das, N., 2024. A new Eosin Y-based 'turnon' fluorescent sensor for ratiometric sensing of toxic mercury ion (Hg2+) offering unaided eye detection and its antibacterial activity. Journal of Hazardous Materials 470 134207. https://doi.org/10.1016/j.jhazmat.2024.134207.

[2] Kumari, C., Sain, D., Kumar, A., Nayek, H. P., Debnath, S., Saha, P., Dey, S., 2017. A bis-hydrazone derivative of 2,5-furandicarboxaldehyde with perfect hetero-atomic cavity for selective sensing of Hg(II) and its intracellular detection in living HeLa S3 cell. Sens. Actuators B: Chem. 243 1181-1190. https://doi.org/10.1016/j.snb.2016.12.103.

[3] Jiang, Z. W., Yang, C., Wu, M., Zhang, P., Liu, Y., Gong, X., Wang, Y., 2025. Multifunctional Tb-MOF-based chemosensor for ratiometric fluorescence detection and removal of mercury ions. Microchemical Journal 214 114088. https://doi.org/10.1016/j.microc.2025.114088.

[4] Hu, J., Hu, Z., Cui, Y., Zhang, X., Gao, H.-W., Uvdal, K., 2014. A rhodamine-based fluorescent probe for Hg^{2+} and its application for biological visualization. Sens. Actuators B: Chem. 203 452-458. https://doi.org/10.1016/j.snb.2014.06.104.

[5] Shi, W., Ma, H., 2008. Rhodamine B thiolactone: a simple chemosensor for Hg^{2+} in aqueous media. Chem. Commun. 1856-1858. 10.1039/B717718F.

[6] Guo, X., Li, L., Wang, L., Yang, M., Wang, Y., Zhang, M., Jia, M., 2025. A paper-based ratiometric sensor for mercury (II) detection using fluorescent carbon dots. Talanta 293 128036. https://doi.org/10.1016/j.talanta.2025.128036.

[7] Lee, H. Y., Swamy, K. M. K., Jung, J. Y., Kim, G., Yoon, J., 2013. Rhodamine hydrazone derivatives based selective fluorescent and colorimetric chemodosimeters for Hg^{2+} and selective colorimetric chemosensor for Cu^{2+}. Sens. Actuators B: Chem. 182 530-537. https://doi.org/10.1016/j.snb.2013.03.050.

[8] Oguz, M., Aydin, D., Malkondu, S., Erdemir, S., 2025. Specific and low-level detection of Hg2+ and CN- in aqueous solution by a new fluorescent probe: Its real sample applications including cell, soil, water, and food. Sensors and Actuators B: Chemical 433 137527. https://doi.org/10.1016/j.snb.2025.137527.

[9] Kaewnok, N., Sirirak, J., Jungsuttiwong, S., Wongnongwa, Y., Kamkaew, A., Petdum, A., Panchan, W., Sahasithiwat, S., Sooksimuang, T., Charoenpanich, A., Wanichacheva, N., 2021. Detection of hazardous mercury ion using [5]helicene-based fluorescence probe with "TurnON" sensing response for practical applications. J. Hazard. Mater. 418 126242. https://doi.org/10.1016/j.jhazmat.2021.126242.

[10] Wang, L., Ma, Y., Lin, W., 2024. A coumarin-based fluorescent probe for highly selective detection of hazardous mercury ions in living organisms. J. Hazard. Mater. 461 132604. https://doi.org/10.1016/j.jhazmat.2023.132604.

[11] Liu, S., Zhang, X., Yan, C., Zhou, P., Zhang, L., Li, Q., Zhang, R., Chen, L., Zhang, L., 2022. A small molecule fluorescent probe for mercury ion analysis in broad low pH range: Spectral, optical mechanism and application studies. J. Hazard. Mater. 424 127701. https://doi.org/10.1016/j.jhazmat.2021.127701.